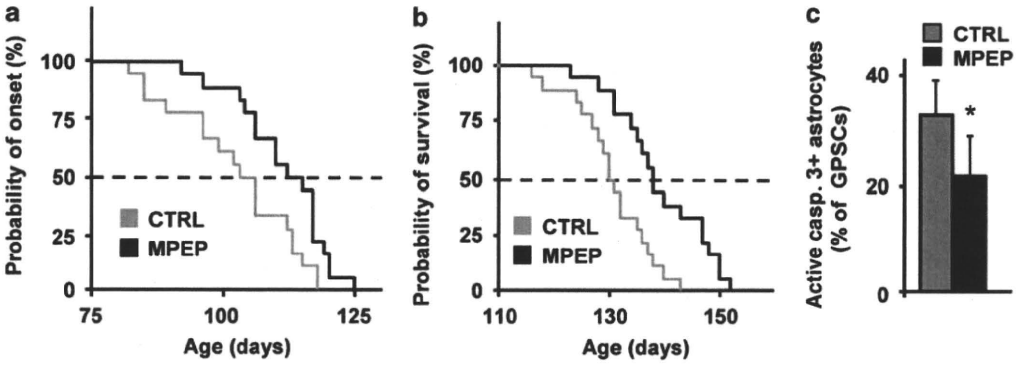

Figure 7 Treatment of hSOD1^{G93A} mice with the mGluR5 antagonist MPEP delays disease onset, extends survival and slows down astrocytic degeneration. (**a** and **b**) Kaplan–Meier curves represent the ages at which the disease onset (peak body weight) (**a**) and death (**b**) were reached for saline-treated (CTRL) and MPEP-treated (MPEP, 30 mg/kg i.p. daily) hSOD1^{G93A} mice ($n=18$ mice for each condition). The dotted line indicates the median values in the two mouse populations. Notice that the onset of symptoms in the MPEP-treated population is significantly retarded by 9 days compared to the CTRL one ($P<0.05$; Logrank test) and life span is extended of 7 days ($P<0.01$; Logrank test). (**c**) Histograms indicate the percentage of spheroid GFAP-positive cells (SGPCs) that are active caspase-3-positive in sections from the end-stage saline-treated (CTRL) or MPEP-treated hSOD1^{G93A} mice ($n=6$ mice for each condition). The number of caspase-3-positive cells is significantly lower in the MPEP-treated group (*$P<0.05$; unpaired *t*-test)

102.4 ± 2.7 days; MPEP: 111.4 ± 2.1, days; Figure 7a). In addition, the mean survival in hSOD1^{G93A} mice treated with MPEP (138.2 ± 2.1 days) was slightly but significantly increased compared to hSOD1^{G93A} mice treated with saline (130.6 ± 1.7 days, Figure 7b). Therefore, these results prove the effectiveness of blocking the mGluR5 receptor *in vivo*.

To investigate whether the effects of MPEP on disease progression correlated to the focal degenerative process of astrocytes, we counted SGPCs in the ventral horns of control and MPEP-treated hSOD1^{G93A} mice at the end stage. While the total number of SGPCs was not statistically different in the two groups of animals (saline: 285 ± 34; MPEP: 258 ± 45), we found a significantly lower number of SGPCs positive for active caspase-3 in the MPEP-treated animals (saline: 93 ± 19; MPEP: 56 ± 19; Figure 7c), suggestive of a less advanced stage of astrocytic degeneration.

Discussion

An increasing body of evidence indicates that degeneration of motor neurons in ALS derives from both cell-autonomous and non-cell-autonomous processes, requiring alterations in motor neurons as well as in the surrounding nonneuronal cells, particularly microglia and astrocytes.[6] An important role for mutant hSOD1 expression in these glial cell types was recently demonstrated in hSOD1^{G37R} transgenic mice by gene excision experiments. Selective reduction of mutant hSOD1 expression in microglia slowed down the late phase of the disease.[7] Moreover, diminished expression of hSOD1 in astrocytes delayed the disease progression.[8]

The specific mechanisms by which glial cells contribute to motor neuron degeneration, however, remain elusive. Astrocytes are known to react to a variety of pathological conditions with a vigorous activation. Moreover, in ALS, they could potentially affect motor neurons in several ways, by the production of toxic species,[10,11] the concurrence to the development of excitotoxicity[12,13] and the modulation of the microglial inflammatory response.[8]

To gain further insights into the contribution of astrocytes to motor neuron degeneration, we analyzed the morphological abnormalities developed by astrocytes during ALS progression in hSOD1^{G93A} mice. By visualizing astrocytes with GFAP staining, we confirmed massive activation of astroglia throughout the spinal cord in the gray and white matter. However, we also identified a degenerative process involving a subset of astrocytes strictly confined to the microenvironment of motor neuron cell bodies, that is within the area of influence of their dendritic trees.[22] The affected cells showed unusual spheroid morphology and most of them lacked the typical GFAP-positive processes. Noteworthy, all SGPCs were strongly immunopositive for ubiquitin. This, in association with the recently described proteasome failure in the lumbar spinal cord of hSOD1^{G93A} mice,[23] may be indicative of alterations of the degradative pathways with the consequent accumulation of ubiquitinated misfolded protein inclusions within the cells. The fact that ubiquitin partially colocalizes with GFAP suggests a direct interaction between the two proteins. Thus, we deduce that GFAP is likely part of the protein aggregates, a condition which may explain the cytoskeletal disorganization identified in this subpopulation of astrocytes. At late time points, part of the SGPCs became immunopositive for active caspase-3. Importantly, a putative caspase-3 cleavage consensus DLTD^{263} site (DLTD^{266} in the human sequence) was recently identified within the GFAP amino acid sequence.[19] Cleavage in this position with generation of a 20 kDa GFAP carboxy-terminal fragment was reported in degenerating astrocytes in Alzheimer's disease.[19] Thus, we investigated whether active caspase-3 acted on the astrocytic cytoskeleton in the spinal cord of hSOD1^{G93A} transgenic mice. Using an antibody that recognizes the carboxy-terminal domain of GFAP, we could confirm that recombinant caspase-3 cleaves GFAP *in vitro* in nontransgenic tissues. Moreover, we detected the typical 20 kDa C-terminal fragment in the transgenic ones. Therefore, we propose that the reduced thickness of the GFAP cap and the reduced number of GFAP-positive processes in the caspase-3-positive SGPCs result from caspase-3-mediated cleavage of the astrocytic

GFAP cytoskeleton. To correlate the degenerative process identified in astrocytes with that in motor neurons, we then evaluated the time-course of appearance of SGPCs. Interestingly, we observed the first ubiquitin-positive SGPCs at 75 days of age, that is before the loss of motor cells. From that time point on, SGPC formation progressed exponentially in parallel to motor neuron degeneration. Therefore, SGPC formation has the potential to contribute to motor neuron decline and to the onset of the symptomatic phase of ALS.

Since the ventral horn gray matter presents a great abundance of excitatory afferents,[20] we decided to investigate how SGPCs interface with glutamatergic nerve terminals in the spinal cord.

In various areas of the brain, astrocytes are intimately associated with synapses, and their perisynaptic processes constitute an anatomical-functional unit, together with the presynaptic and postsynaptic elements, dubbed 'the tripartite synapse'.[24] This strategic location allows astrocytes to sense and respond to neurotransmitter spilled out of the synaptic cleft during neuronal activity.[25] Thus, glutamate released from excitatory presynapses during transmission can activate its receptors in the perisynaptic astrocytic processes and trigger neuron-glia signaling.[26,27] In addition to glial activation by synaptic spillover, there is also evidence for direct neuron-glia communication. This can occur either through the release of transmitter from presynaptic 'ectopic sites' directly facing glia,[28] or through the specific neuron-glia synaptic junctions that connect excitatory or inhibitory nerve terminals to the so-called 'NG2-glia', a peculiar type of glial cells immunopositive for the proteoglycan NG2.[29] Interestingly, studies on transgenic mice identified a group of brain cells expressing both NG2 and astrocytic markers.[30] We clearly do not know whether SGPCs derive from this population and receive direct neuronal input. This would be an attractive explanation for their selective vulnerability, but further investigations are necessary to clarify this possibility.

A number of observations indicates that glutamate handling is altered in both sporadic human ALS cases and mutant hSOD1-expressing transgenic mice, particularly due to the loss of the astrocytic glutamate transporter EAAT2/GLT1.[3,4,13]

Motor cells are potentially highly vulnerable to changes in extracellular glutamate levels as they express a large number of calcium-permeable AMPA receptors[12,31–33] and have limited capacity to buffer calcium.[34] Although astrocytes express functional glutamate receptors, they are normally more resistant to stimuli that are excitotoxic for neurons. However, in this study, we found that cultured astrocytes that express hSOD1^{G93A} or hSOD1^{G85R} become susceptible to concentrations of exogenous glutamate that are not detrimental for wild-type astrocytes.[21] Moreover, they degenerate in response to a moderate increase (about 2 μM) of the endogenous ambient glutamate, induced by the uptake inhibitor TBOA. Such a glutamate concentration is reached at the astrocytic membrane during the normal excitatory neurotransmission and starts glutamate receptor-mediated intracellular signaling in astrocytes.[27] Thus, it is possible that the defects of glutamate uptake in ALS – the situation mimicked by TBOA – prolong activation of astrocytic glutamate receptors and amplify the deleterious process. Noteworthy, SGPCs resulted very weakly immunopositive for EAAT2/GLT1, suggesting a reduction of the transporter expression on these cells. A role for the metabotropic glutamate receptors in ALS was previously postulated by others.[35,36] Our data add further insight into this finding by indicating that the phenomenon herein identified, that is glutamate-dependent degeneration of mutant hSOD1-expressing astrocytes, is specifically mediated by mGluR5 *in vitro*. This finding is particularly interesting in view of previous observations highlighting mGluR5 abnormalities in ALS. Indeed, the expression of mGluR5 in the ventral spinal cord of ALS patients was reported to be selectively upregulated in astrocytes.[37] Moreover, astrocytes from hSOD1^{G93A} rats display enhanced mGluR5 expression accompanied by alterations of the coupled signal-transduction pathways.[38] The potential relevance of our observations to ALS pathogenesis was confirmed by the studies *in vivo*. These showed that MPEP controls, at least in part, the degenerative process of astrocytes, reducing the number of caspase-3-positive SGPCs. In parallel, administration of MPEP delays motor decline and extends the survival of hSOD1^{G93A} transgenic mice.

In conclusion, this study shows that a subpopulation of spinal astrocytes undergoes a degenerative process in ALS. This phenomenon is most likely relevant in the context of ALS pathogenesis because: (a) it is spatially restricted to astrocytes located in the microenvironment of motor neurons; (b) it starts when most motor neurons, although suffering,[39] are still alive; (c) it is sensitive to mGluR5 blockage *in vivo*. These observations suggest a scenario where distressed motor neurons affect the health conditions of adjacent astrocytes. Astrocytes, weakened by the expression of mutant hSOD1, become vulnerable to stimuli, such as glutamate, present in their microenvironment, and start to degenerate. This in turn may accelerate degeneration of the neighboring motor cells in an interactive process of reciprocal damage. In this context, our data complement and extend the excitotoxic hypothesis in ALS, introducing the concept that glutamatergic alterations are noxious not only to motor neurons but also to the associated astrocytes. In particular, we identify for the first time a 'gliotoxic' role of mGluR5 and a protective action of mGluR5 antagonists. This finding opens perspectives for new therapeutic approaches where mGluR5 inhibition can be combined to treatments acting on complementary mechanisms and cell targets.

Materials and Methods

Transgenic mice. Transgenic mice expressing the human SOD1^{G93A} (B6SJL-TgN(SOD1-G93A)1Gur or the human SOD1^{WT} (B6SJL-Tg(SOD1)2Gur/J)[2] were purchased from The Jackson Laboratories. The colonies were maintained by breeding hemizygote males to wild-type C57Bl6/SJL hybrid females (Charles River Laboratories). Offspring were genotyped and used for subsequent studies.

Histological analysis. Mice were transcardially perfused with 4% buffered paraformaldehyde and spinal cords were postfixed in the same solution. The lumbar tract was removed, paraffin embedded and sectioned at 10 μm. On selected sections, the following immunohistochemical stainings were carried out: GFAP as astrocytic marker (mouse monoclonal antibody, 1:25, Dako; rabbit polyclonal antibody, 1:1000, Dako; mouse Alexa fluor 488 conjugated monoclonal antibody, 1:1000, Chemicon), nonphosphorylated neurofilament H as neuronal marker (SMI32, mouse monoclonal antibody, 1:500, Sternberger Monoclonals Incorporated), synaptophysin (clone SY38, mouse monoclonal antibody, 1:100, Dako), VGLUT1 (rabbit polyclonal antibody, 1:3000, Synaptic Systems; rabbit polyclonal antibody fluorescence-labeled with Oyster 550, 1:1500, Synaptic

Systems), EAAT1/GLAST and EAAT2/GLT1 (rabbit polyclonal antibodies, 0.6 and 0.4 μg/ml, respectively), active caspase-3 (rabbit polyclonal antibody, 1:50, Cell Signalling), ubiquitin (rabbit polyclonal antibody, 1:300, Dako). To detect active caspase-3, a Tyramide Amplification System kit was used (NEN). For histopathological analysis, serial sections were immunostained for GFAP/ubiquitin or GFAP/active caspase-3 and positive astrocytes were counted for a total of 8–10 disectors using an unbiased stereologic physical disector technique.

Z-axis image stacks (z-step size: 0.4 μm) were collected to generate three-dimensional data sets of spinal cord sections on a Bio-Rad Radiance 2100 confocal microscope with a 60× Planapo NA1,4 oil-immersion objective in condition of optimal iris diameter as defined by LaserSharp 2000 software. To determine the spatial relationship between spheroid astrocytes and the neighboring motor neurons, image stacks were sectioned along the Z-axis using ImageJ software (National Institutes of Health) and the interdistance between the periphery of GFAP staining and the boundary of motor neuron cell body, as defined by SMI32 staining, was measured within 200 μm in spinal cord sections from 100-day-old mice. Distances were put into bins of 10 μm and their frequency of distribution were calculated.

Quantitative analysis of punctuate staining of VGLUT1 and synaptophysin was performed on images of the ventral horns of double stained sections from the mouse lumbar spinal cord. Five random 20 × 20 μm fields per each image were processed using the colocalization plugin of ImageJ software.

Caspase-3-dependent cleavage reaction. Spinal cord homogenates (10%) from end stage hSOD1^{G93A} mice or age-matched wild-type littermates were prepared in PBS containing 1% CHAPS and protease inhibitors (Complete Mini, Roche). Homogenates were centrifuged at 400× *g* for 10 min, supernatants were removed and stored at −80 °C.

For caspase-cleavage experiments, 20 μg of total protein were incubated for 4 h at 37 °C in cleavage buffer (50 mM Hepes pH 7.2, 50 mM NaCl, 10 mM EDTA, 0.1% CHAPS, 5% glycerol, 10 mM DTT) in the absence or in the presence of increasing concentrations of recombinant active caspase-3 (Calbiochem). Reactions were terminated by adding SDS-containing sample buffer (50 mM TrisHCl pH 6.8, 2% (w/v) SDS, 10% (v/v) glycerol, 100 mM DTT, 4% β-mercaptoethanol, 0.1% (w/v) bromophenol blue) and boiling for 10 min.

Western blot analysis. Caspase-cleaved tissues or cell lysates were electrophoresed through 10% SDS-polyacrylamide gels and transferred to nitrocellulose membranes. GFAP was detected with a mouse monoclonal antibody (clone G-A-5), which recognizes the carboxy-teminal domain of GFAP (1:500, Chemicon). EAAT1/GLAST and EAAT2/GLT1 were detected using rabbit polyclonal antibodies (0.2 and 0.1 μg/ml, respectively). β-actin was detected with a mouse monoclonal antibody (clone AC-15; 1:3000, Sigma).

Astrocyte cultures and transfection. Primary astrocyte cultures (>99% GFAP-positive) were prepared from the spinal cord of newborn mice (hSOD1^{G93A}, hSOD1^{WT} or nontransgenic littermates) or rats (wild-type) as described previously,[40] plated at a density of 8×10^4 cells/well in 24-well plates containing glass coverslips and maintained in minimal essential medium (MEM) supplemented with 10% fetal calf serum. Confluent mouse cultures were directly used for experiments with pharmacological challenges. Rat spinal cord astrocytes were transfected 24 h after plating with the marker plasmid pEGFP-C3 (0.5 μg, Clontech Laboratories) in combination with expression vectors coding for either wild-type or mutant (G85R or G93A) c-Myc-tagged hSOD1s (1 μg). Transfection was performed with FuGENE6 Transfection Reagent (Roche). Immunocytochemical stainings using a monoclonal anti-Human c-Myc antibody (1:200, BD Biosciences Pharmingen) revealed that EGFP and c-Myc-tagged proteins colocalize in 95% of cases.

hSOD1 expression levels were determined on transfected astrocytes immunostained for c-Myc by immunofluorescence quantification as follows. Average fluorescence intensity from transfected astrocytes was measured and expressed as fluorescence intensity arbitrary units on a linear scale of 0–256 in nonsaturating condition of the camera, using the ImageJ software. Fluorescence intensity values were then expressed relative to mean fluorescence intensity obtained from the nontransfected cells (background noise).

No significant difference in the expression levels was detected between the wild-type and the mutant proteins (hSOD1^{WT} expression level was set as 100%; hSOD1^{G93A}: 123 ± 13.1% *versus* hSOD1^{WT}; hSOD1^{G85R}: 116.4 ± 11.8% *versus* hSOD1^{WT}; $n = 50$ cells/genotype; values represent the mean ± S.E.M. of three independent experiments; $P = 0.46$, one-way ANOVA). Pharmacological experiments were carried out 48 h after transfection.

Expression of the glutamate transporters EAAT1/GLAST and EAAT2/GLT1 was evaluated on astrocyte cultures fixed with 4% buffered paraformaldehyde. EAAT1/GLAST and EAAT2/GLT1 were detected using rabbit polyclonal antibodies (0.5 and 1 μg/ml, respectively). GFAP was detected with a mouse monoclonal antibody (clone G-A-5, 1:200, Chemicon).

Pharmacological treatments *in vitro*. Astrocyte cultures were exposed to one or combinations of the following agents for 30 min: L-Glutamate (500 μM), CNQX (10 μM), MCPG (500 μM) MPEP (200 nM), GYKI 52466 (50 μM), DHPG (100 μM), TBOA (200 μM). All agents were from Tocris Bioscience, except L-Glutamate, from Sigma. After removal of the agents, astrocytes were allowed to recover at 37 °C for 24 h.

Astrocyte toxicity assays. The toxic effect of pharmacological treatments to astrocytes in culture was determined by double staining with the fluorescent nuclear dye Hoechst 33342 (Sigma) and anti-active caspase-3 immunocytochemistry using a rabbit polyclonal antibody (Cell Signalling). The number of astrocytes showing condensed nuclei and active caspase-3 24 h after the pharmacological challenge was counted in a blind manner by two independent operators. For mouse cultures, the number of dying astrocytes was counted in 8–10 microscopic fields (40 ×) per coverslip and expressed as percentage of the total number of cells present in the field. For transfected rat astrocytes, it was expressed as percentage of the total number of transfected cells (EGFP-positive) present in the coverslip. In each experiment, 2–3 coverslips/condition were counted and experiments were replicated as indicated in the legends.

Extracellular glutamate concentration in the astrocyte cultures. Endogenous glutamate accumulated in the supernatant of astrocytes incubated with TBOA 200 μM for 30 min was measured by a specific enzymatic assay, as described previously.[40] Briefly, cell supernatant was introduced in a 1 × 1 cm cuvette (Hellma Italia) inside a LS55 computerized spectrofluorometer (Perkin-Elmer) at 37 °C under continuous stirring in a buffer containing (in mM): NaCl 120, KCl 3.1, NaH_2PO_4 1.25, HEPES-Na 25, $MgCl_2$ 1, glucose 4, $CaCl_2$ 2 at pH 7.4, added with glutamate dehydrogenase (GDH, 15.5 U/ml) and 1 mM $NADP^+$. Glutamate present in the cell medium was oxidized by GDH to α-ketoglutarate with the formation of NADPH and fluorescence emission at 430 nm (excitation light 335 nm). Glutamate was quantified referring to the standard curves constructed with exogenous glutamate.

Pharmacological treatments *in vivo*. hSOD1^{G93A} mice were administered daily 30 mg/kg MPEP or saline intraperitoneally starting at the age of 40 days ($n = 18$ mice for each condition). Mice were thereafter kept under daily observation and weighted once a week. Since decline in peak body weight is considered the earliest observable measure of disease onset and strictly correlates with decline in motor performance,[7,8] the onset of clinical disease was defined by the achievement of peak body weight. End stage was defined as the time at which animals were unable to right themselves within 30 s when placed on their side.

Acknowledgements. We are grateful to P Caroni, P Clarke and J Meldolesi for scientific discussions and advice; NC Danbolt for providing the anti-GLT1 and anti-GLAST antibodies; P Bezzi, S Vesce and V Schubert for critical reading and comments on the manuscript; GE Rovati e G Gambino for statistical advice; C Cafè and D Scirea for contributions in the early phases of this study; G Biondi, F Niccolini and F Martorana for experimental help; G Simonutti for technical assistance with confocal microscopy. This work was supported by a grant from Fondazione Telethon (GGP05244) and an EMBO long-term fellowship (ALTF 279-2002) to DR and by grants from Fondazione Telethon (GGP02052), Fondazione Cariplo, Ministero Italiano della Università e Ricerca (COFIN, FIRB, FIRST) to AV.

1. Rosen DR, Siddique T, Patterson D, Figlewicz DA, Sapp P, Hentati A *et al.* Mutations in Cu/Zn superoxide dismutase gene are associated with familial amyotrophic lateral sclerosis. *Nature* 1993; **362**: 59–62.
2. Gurney ME, Pu H, Chiu AY, Dal Canto MC, Polchow CY, Alexander DD *et al.* Motor neuron degeneration in mice that express a human Cu,Zn superoxide dismutase mutation. *Science* 1994; **264**: 1772–1775.

3. Bruijn LI, Becher MW, Lee MK, Anderson KL, Jenkins NA, Copeland NG *et al.* ALS-linked SOD1 mutant G85R mediates damage to astrocytes and promotes rapidly progressive disease with SOD1-containing inclusions. *Neuron* 1997; **18**: 327–338.
4. Howland DS, Liu J, She Y, Goad B, Maragakis NJ, Kim B *et al.* Focal loss of the glutamate transporter EAAT2 in a transgenic rat model of SOD1 mutant-mediated amyotrophic lateral sclerosis (ALS). *Proc Natl Acad Sci USA* 2002; **99**: 1604–1609.
5. Jaarsma D, Teuling E, Haasdijk ED, De Zeeuw CI, Hoogenraad CC. Neuron-specific expression of mutant superoxide dismutase is sufficient to induce amyotrophic lateral sclerosis in transgenic mice. *J Neurosci* 2008; **28**: 2075–2088.
6. Clement AM, Nguyen MD, Roberts EA, Garcia ML, Boillee S, Rule M *et al.* Wild-type nonneuronal cells extend survival of SOD1 mutant motor neurons in ALS mice. *Science* 2003; **302**: 113–117.
7. Boillee S, Yamanaka K, Lobsiger CS, Copeland NG, Jenkins NA, Kassiotis G *et al.* Onset and progression in inherited ALS determined by motor neurons and microglia. *Science* 2006; **312**: 1389–1392.
8. Yamanaka K, Chun SJ, Boillee S, Fujimori-Tonou N, Yamashita H, Gutmann DH *et al.* Astrocytes as determinants of disease progression in inherited amyotrophic lateral sclerosis. *Nat Neurosci* 2008; **11**: 251–253.
9. Beers DR, Henkel JS, Xiao Q, Zhao W, Wang J, Yen AA *et al.* Wild-type microglia extend survival in PU.1 knockout mice with familial amyotrophic lateral sclerosis. *Proc Natl Acad Sci USA* 2006; **103**: 16021–16026.
10. Nagai M, Re DB, Nagata T, Chalazonitis A, Jessell TM, Wichterle H *et al.* Astrocytes expressing ALS-linked mutated SOD1 release factors selectively toxic to motor neurons. *Nat Neurosci* 2007; **10**: 615–622.
11. Di Giorgio FP, Carrasco MA, Siao MC, Maniatis T, Eggan K. Non-cell autonomous effect of glia on motor neurons in an embryonic stem cell-based ALS model. *Nat Neurosci* 2007; **10**: 608–614.
12. Van Damme P, Bogaert E, Dewil M, Hersmus N, Kiraly D, Scheveneels W *et al.* Astrocytes regulate GluR2 expression in motor neurons and their vulnerability to excitotoxicity. *Proc Natl Acad Sci USA* 2007; **104**: 14825–14830.
13. Rothstein JD, Van Kammen M, Levey AI, Martin LJ, Kuncl RW. Selective loss of glial glutamate transporter GLT-1 in amyotrophic lateral sclerosis. *Ann Neurol* 1995; **38**: 73–84.
14. Guo H, Lai L, Butchbach ME, Stockinger MP, Shan X, Bishop GA *et al.* Increased expression of the glial glutamate transporter EAAT2 modulates excitotoxicity and delays the onset but not the outcome of ALS in mice. *Hum Mol Genet* 2003; **12**: 2519–2532.
15. Rothstein JD, Patel S, Regan MR, Haenggeli C, Huang YH, Bergles DE *et al.* Beta-lactam antibiotics offer neuroprotection by increasing glutamate transporter expression. *Nature* 2005; **433**: 73–77.
16. Pardo AC, Wong V, Benson LM, Dykes M, Tanaka K, Rothstein JD *et al.* Loss of the astrocyte glutamate transporter GLT1 modifies disease in SOD1(G93A) mice. *Exp Neurol* 2006; **201**: 120–130.
17. Pasinelli P, Houseweart MK, Brown Jr RH, Cleveland DW. Caspase-1 and -3 are sequentially activated in motor neuron death in Cu,Zn superoxide dismutase-mediated familial amyotrophic lateral sclerosis. *Proc Natl Acad Sci USA* 2000; **97**: 13901–13906.
18. Chiu AY, Zhai P, Dal Canto MC, Peters TM, Kwon YW, Prattis SM *et al.* Age-dependent penetrance of disease in a transgenic mouse model of familial amyotrophic lateral sclerosis. *Mol Cell Neurosci* 1995; **6**: 349–362.
19. Mouser PE, Head E, Ha KH, Rohn TT. Caspase-mediated cleavage of glial fibrillary acidic protein within degenerating astrocytes of the Alzheimer's disease brain. *Am J Pathol* 2006; **168**: 936–946.
20. Alvarez FJ, Villalba RM, Zerda R, Schneider SP. Vesicular glutamate transporters in the spinal cord, with special reference to sensory primary afferent synapses. *J Comp Neurol* 2004; **472**: 257–280.
21. Choi DW, Maulucci-Gedde M, Kriegstein AR. Glutamate neurotoxicity in cortical cell culture. *J Neurosci* 1987; **7**: 357–368.
22. Inglis FM, Furia F, Zuckerman KE, Strittmatter SM, Kalb RG. The role of nitric oxide and NMDA receptors in the development of motor neuron dendrites. *J Neurosci* 1998; **18**: 10493–10501.
23. Kabashi E, Agar JN, Taylor DM, Minotti S, Durham HD. Focal dysfunction of the proteasome: a pathogenic factor in a mouse model of amyotrophic lateral sclerosis. *J Neurochem* 2004; **89**: 1325–1335.
24. Araque A, Parpura V, Sanzgiri RP, Haydon PG. Tripartite synapses: glia, the unacknowledged partner. *Trends Neurosci* 1999; **22**: 208–215.
25. Volterra A, Meldolesi J. Astrocytes, from brain glue to communication elements: the revolution continues. *Nat Rev Neurosci* 2005; **6**: 626–640.
26. Pasti L, Volterra A, Pozzan T, Carmignoto G. Intracellular calcium oscillations in astrocytes: a highly plastic, bidirectional form of communication between neurons and astrocytes *in situ*. *J Neurosci* 1997; **17**: 7817–7830.
27. Wang X, Lou N, Xu Q, Tian GF, Peng WG, Han X *et al.* Astrocytic Ca2+ signaling evoked by sensory stimulation *in vivo*. *Nat Neurosci* 2006; **9**: 816–823.
28. Matsui K, Jahr CE. Exocytosis unbound. *Curr Opin Neurobiol* 2006; **16**: 305–311.
29. Paukert M, Bergles DE. Synaptic communication between neurons and NG2+ cells. *Curr Opin Neurobiol* 2006; **16**: 515–521.
30. Matthias K, Kirchhoff F, Seifert G, Huttmann K, Matyash M, Kettenmann H *et al.* Segregated expression of AMPA-type glutamate receptors and glutamate transporters defines distinct astrocyte populations in the mouse hippocampus. *J Neurosci* 2003; **23**: 1750–1758.
31. Williams TL, Day NC, Ince PG, Kamboj RK, Shaw PJ. Calcium-permeable alpha-amino-3-hydroxy-5-methyl-4-isoxazole propionic acid receptors: a molecular determinant of selective vulnerability in amyotrophic lateral sclerosis. *Ann Neurol* 1997; **42**: 200–207.
32. Van Damme P, Van Den Bosch L, Van Houtte E, Callewaert G, Robberecht W. GluR2-dependent properties of AMPA receptors determine the selective vulnerability of motor neurons to excitotoxicity. *J Neurophysiol* 2002; **88**: 1279–1287.
33. Kawahara Y, Ito K, Sun H, Aizawa H, Kanazawa I, Kwak S. Glutamate receptors: RNA editing and death of motor neurons. *Nature* 2004; **427**: 801.
34. Alexianu ME, Ho BK, Mohamed AH, La Bella V, Smith RG, Appel SH. The role of calcium-binding proteins in selective motoneuron vulnerability in amyotrophic lateral sclerosis. *Ann Neurol* 1994; **36**: 846–858.
35. Anneser JM, Borasio GD, Berthele A, Zieglgansberger W, Tolle TR. Differential expression of group I metabotropic glutamate receptors in rat spinal cord somatic and autonomic motoneurons: possible implications for the pathogenesis of amyotrophic lateral sclerosis. *Neurobiol Dis* 1999; **6**: 140–147.
36. Anneser JM, Chahli C, Borasio GD. Protective effect of metabotropic glutamate receptor inhibition on amyotrophic lateral sclerosis-cerebrospinal fluid toxicity *in vitro*. *Neuroscience* 2006; **141**: 1879–1886.
37. Aronica E, Catania MV, Geurts J, Yankaya B, Troost D. Immunohistochemical localization of group I and II metabotropic glutamate receptors in control and amyotrophic lateral sclerosis human spinal cord: upregulation in reactive astrocytes. *Neuroscience* 2001; **105**: 509–520.
38. Vermeiren C, Hemptinne I, Vanhoutte N, Tilleux S, Maloteaux JM, Hermans E. Loss of metabotropic glutamate receptor-mediated regulation of glutamate transport in chemically activated astrocytes in a rat model of amyotrophic lateral sclerosis. *J Neurochem* 2006; **96**: 719–731.
39. Pun S, Santos AF, Saxena S, Xu L, Caroni P. Selective vulnerability and pruning of phasic motoneuron axons in motoneuron disease alleviated by CNTF. *Nat Neurosci* 2006; **9**: 408–419.
40. Bezzi P, Domercq M, Brambilla L, Galli R, Schols D, De Clercq E *et al.* CXCR4-activated astrocyte glutamate release via TNFalpha: amplification by microglia triggers neurotoxicity. *Nat Neurosci* 2001; **4**: 702–710.

Supplementary Information accompanies the paper on Cell Death and Differentiation website (http://www.nature.com/cdd)

ALS-linked mutant SOD1 induces ER stress- and ASK1-dependent motor neuron death by targeting Derlin-1

Hideki Nishitoh, Hisae Kadowaki, Atsushi Nagai, et al.

Genes Dev. 2008 22: 1451-1464
Access the most recent version at doi:10.1101/gad.1640108

ALS-linked mutant SOD1 induces ER stress- and ASK1-dependent motor neuron death by targeting Derlin-1

Hideki Nishitoh,[1,2,3] Hisae Kadowaki,[1,2,3,4,5] Atsushi Nagai,[3] Takeshi Maruyama,[3] Takanori Yokota,[6] Hisashi Fukutomi,[1,4,5] Takuya Noguchi,[1,4,5] Atsushi Matsuzawa,[1,4,5] Kohsuke Takeda,[1,4,5] and Hidenori Ichijo[1,4,5,7]

[1]Core Research for Evolutional Science and Technology (CREST), Japan Science and Technology Corporation, Bunkyo-ku, Tokyo 113-0033, Japan; [2]Oral and Maxillofacial Surgery, Graduate School, Tokyo Medical and Dental University, Bunkyo-ku, Tokyo 113-8510, Japan; [3]Center of Excellence Program for Frontier Research on Molecular Destruction and Reconstruction of Tooth and Bone, Tokyo Medical and Dental University, Bunkyo-ku, Tokyo 113-8510, Japan; [4]Cell Signaling, Graduate School of Pharmaceutical Sciences, The University of Tokyo, Bunkyo-ku, Tokyo 113-0033, Japan; [5]Strategic Approach to Drug Discovery and Development in Pharmaceutical Sciences, Center of Excellence Program, Bunkyo-ku, Tokyo 113-0033, Japan; [6]Department of Neurology and Neurological Science, Graduate School, Tokyo Medical and Dental University, Bunkyo-ku, Tokyo 113-8519, Japan

Mutation in *Cu/Zn-superoxide dismutase* (*SOD1*) is a cause of familial amyotrophic lateral sclerosis (ALS). Mutant SOD1 protein (SOD1^{mut}) induces motor neuron death, although the molecular mechanism of SOD1^{mut}-induced cell death remains controversial. Here we show that SOD1^{mut} specifically interacted with Derlin-1, a component of endoplasmic reticulum (ER)-associated degradation (ERAD) machinery and triggered ER stress through dysfunction of ERAD. SOD1^{mut}-induced ER stress activated the apoptosis signal-regulating kinase 1 (ASK1)-dependent cell death pathway. Perturbation of binding between SOD1^{mut} and Derlin-1 by Derlin-1-derived oligopeptide suppressed SOD1^{mut}-induced ER stress, ASK1 activation, and motor neuron death. Moreover, deletion of *ASK1* mitigated the motor neuron loss and extended the life span of SOD1^{mut} transgenic mice. These findings demonstrate that ER stress-induced ASK1 activation, which is triggered by the specific interaction of Derlin-1 with SOD1^{mut}, is crucial for disease progression of familial ALS.

[*Keywords*: Amyotrophic lateral sclerosis; endoplasmic reticulum-associated degradation; endoplasmic reticulum stress; Derlin-1; ASK1]

Supplemental material is available at http://www.genesdev.org.

Received December 5, 2007; revised version accepted April 11, 2008.

Amyotrophic lateral sclerosis (ALS) is the most frequent adult-onset motor neuron disease and is characterized by selective loss of motor neurons. Familial ALS-linked mutations of *Cu/Zn-superoxide dismutase* (*SOD1*) induce motor neuron death. Previous studies have suggested that SOD1^{mut} causes various cellular events, including alteration of gene expression (Yoshihara et al. 2002; Kirby et al. 2005), abnormal protein interactions (Kunst et al. 1997), activation of caspases (Pasinelli et al. 1998; Li et al. 2000), dysfunction of mitochondria (Bowling et al. 1993; Wong et al. 1995; Liu et al. 2004), and cytoskeletal abnormalities (Julien and Beaulieu 2000). However, the causal relationship between these events and motor neuron death remains unclear.

Endoplasmic reticulum (ER) stress is triggered by the accumulation of misfolded proteins within the ER lumen and has recently been implicated in various neurodegenerative diseases (Sekine et al. 2006). Recent studies have suggested that ER stress signaling is also involved in the pathogenesis of ALS (Tobisawa et al. 2003; Atkin et al. 2006; Kikuchi et al. 2006). We showed previously that, upon ER stress, an ER-resident type I transmembrane serine/threonine kinase termed IRE1 recruits TRAF2 and ASK1 (apoptosis signal-regulating kinase 1) on the ER membrane and thus activates the ASK1-dependent apoptosis pathway (Nishitoh et al. 2002). Several groups have reported that activation of the ASK1 cascade is associated with induction of motor neuron death by SOD1^{mut} both in vitro (Raoul et al. 2002) and in vivo (Wengenack et al. 2004; Holasek et al. 2005; Veglianese et al. 2006). These observations suggested that a functional link between ER stress and ASK1 may exist in the process of SOD1^{mut}-induced motor neuron death. However, the molecular mechanism by which SOD1^{mut}

[7]**Corresponding author.**
E-MAIL ichijo@mol.f.u-tokyo.ac.jp; FAX 81-3-5841-4778.
Article is online at http://www.genesdev.org/cgi/doi/10.1101/gad.1640108.

induces ER stress has remained unclear. Furthermore, genetic evidence has not been provided regarding the hypothetical involvement of ER stress–ASK1 pathway in SOD1^{mut}-induced motor neuron death. In the present study, we investigated the molecular mechanism of SOD1^{mut}-induced ER stress and the role of ER stress-induced ASK1 activation in the pathogenesis of ALS.

Results

SOD1^{mut} triggers ER stress

To investigate the causal relationship between SOD1^{mut} and ER stress-dependent motor neuron death, we first examined whether SOD1^{mut} induces ER stress in NSC34 motor neurons, as assessed by band-shift analyses of the ER transmembrane kinase receptors IRE1 and PERK. Adenovirus (Ad)-mediated expression of ALS-linked SOD1^{mut} (SOD1^{G93A}) was detectable within 48 h of infection (Supplemental Fig. S1A). SOD1^{mut} (SOD1^{A4V}, SOD1^{G85R}, and SOD1^{G93A}) but not wild-type SOD1 (SOD1^{wt}) activated IRE1 and PERK (Fig. 1A; Supplemental Fig. S1A). To confirm the activation of IRE1 by SOD1^{mut}, we examined Xbp-1 mRNA splicing by RT–PCR. We clearly observed the appearance of spliced Xbp-1 mRNA by SOD1^{mut} but not SDO1^{wt} in HEK293 cells (Supplemental Fig. S1B) and NSC34 cells (Fig. 4D, lanes 2–5, below). SOD1^{mut}-specific induction of CHOP and BiP (ER stress marker proteins) was also observed (Fig. 1B). These findings suggested that accumulation of various SOD1^{mut} proteins commonly induce ER stress.

Inhibition of proteasome activity has been reported to be induced by SOD1^{mut} in Neuro2a cells (Urushitani et al. 2002). Since polyglutamine (polyQ) fragments have been shown to induce ER stress through inhibition of proteasome activity (Nishitoh et al. 2002), SOD1^{mut} might also induce ER stress through proteasomal dysfunction. We therefore examined whether alteration of proteasome activity was involved in SOD1^{mut}-induced ER stress. Proteasome activity was inhibited by treatment with lactacystin, a proteasome inhibitor, but not by Ad-mediated expression of SOD1^{mut} in NSC34 cells within 48 h (Supplemental Fig. S2A). These findings suggested that a mechanism other than proteasomal dysfunction may be involved in SOD1^{mut}-induced ER stress in NSC34 cells.

SOD1^{mut} inhibits ERAD

Restoration of ER homeostasis is achieved mainly by two independent mechanisms, chaperone-dependent refolding and ER-associated degradation (ERAD). In ERAD, misfolded proteins are exported from the ER back into the cytosol and are rapidly degraded by the ubiquitin–proteasome system (UPS) (Kopito 1997; Tsai et al. 2002; Meusser et al. 2005). Blocking of the refolding mechanism and/or the ERAD mechanism induces accumulation of misfolded proteins within the ER lumen and thus ER stress. Since SOD1^{mut} clearly induced expression of

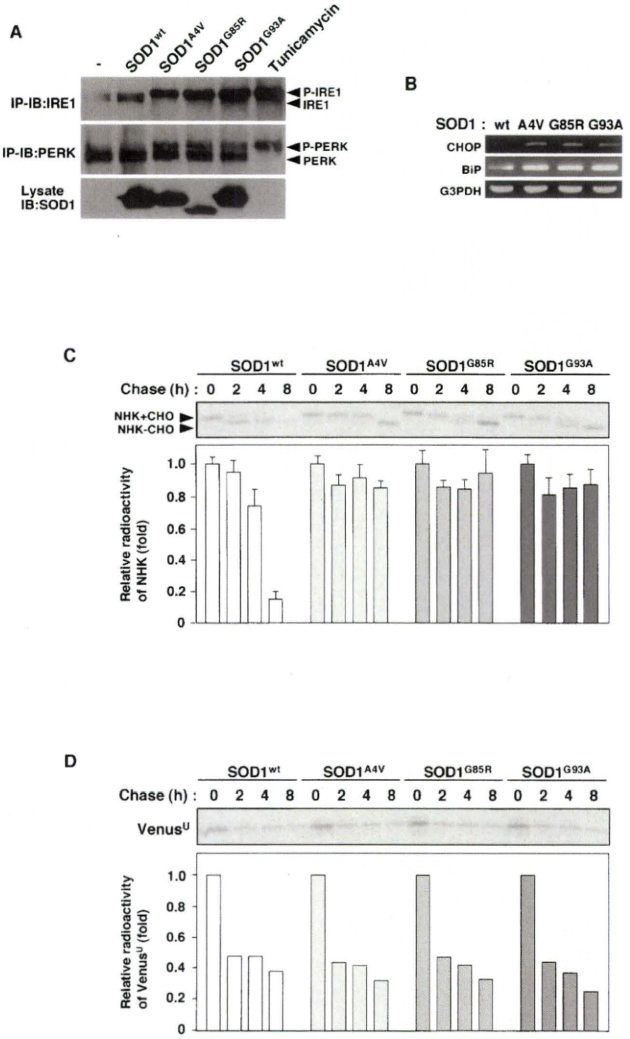

Figure 1. SOD1^{mut} triggers ER stress and inhibition of ERAD. (*A*) NSC34 cells were lysed after infection with Ad-SOD1^{wt}, Ad-SOD1^{A4V}, Ad-SOD1^{G85R}, or Ad-SOD1^{G93A} for 48 h or treatment with 2.5 μg/mL tunicamycin (a potent inducer of ER stress) for 2 h and analyzed by immunoprecipitation-immunoblotting (IP-IB) with antibodies to IRE1α or PERK. (P-IRE1) Activated IRE1; (P-PERK) activated PERK. The presence of SOD1 in the same lysates is shown. (*B*) NSC34 cells were transfected with SOD1^{wt} or SOD1^{mut} for 48 h. Expression of BiP and CHOP was examined by RT–PCR. (*C*) NSC34 cells were transfected with NHK and SOD1^{wt} or SOD1^{mut}. Cells were pulse-labeled with [^{35}S] methionine and cysteine and chased for the indicated time periods. Cell lysates were immunoprecipitated with antibody to α1AT. (NHK + CHO) Glycosylated NHK; (NHK − CHO) deglycosylated NHK. The relative radioactivities in NHK at different times of chase were calculated and are shown as fold decreases relative to the intensity observed at 0 h chase. (*D*) NSC34 cells were transfected with Venus^{U} and SOD1^{wt} or SOD1^{mut}. Cells were pulse-labeled with [^{35}S] methionine and cysteine and chased for the indicated time periods. Cell lysates were immunoprecipitated with antibody to GFP. The relative radioactivities in Venus^{U} at different times of chase were calculated and are shown as fold decreases relative to the intensity observed at 0 h chase.

the ER-resident chaperone BiP (Fig. 1B), the productive refolding mechanism appears not to be inhibited by $SOD1^{mut}$. To examine whether $SOD1^{mut}$ interferes with the ERAD mechanism, we examined the stability of the null Hong Kong (NHK) mutant protein of α1-antitrypsin (α1AT), an ER luminal misfolded protein (Sifers et al. 1988). Pulse-chase experiments showed that NHK was degraded with a half-life of <8 h in NSC34 cells transfected with or without $SOD1^{wt}$ (Fig. 1C; Supplemental Fig. S3A). In contrast, overexpression of $SOD1^{mut}$ decreased the degradation of NHK to a half-life of >8 h (Fig. 1C). To confirm the interference with the degradation of the other ERAD substrate by $SOD1^{mut}$, we examined the stability of CD3δ, a well-characterized transmembrane-type ERAD substrate (Fang et al. 2001). Cycloheximide chase experiments showed that the degradation of CD3δ was also retarded by overexpression of $SOD1^{mut}$ (Supplemental Fig. S3C). To further examine whether $SOD1^{mut}$ also interferes with the degradation of cytosolic protein, we examined the stability of the unstable Venus mutant protein ($Venus^U$), a cytosolic proteasome substrate. There was no difference between a half-life of $Venus^U$ in $SOD1^{wt}$ transfected cells and that in $SOD1^{mut}$ transfected cells (Fig. 1D). These findings suggested that $SOD1^{mut}$ specifically impairs ERAD function but not cytosolic protein degradation in motor neurons. Furthermore, $SOD1^{mut}$ clearly delayed the deglycosylation of NHK in addition to degradation (see the band shift of NHK; Fig. 1C). Previous studies have reported that the cytoplasmic peptide N-glycanase contributes to deglycosylation of misfolded glycoproteins prior to degradation (Suzuki et al. 2002). Thus, the delay of the deglycosylation of NHK suggested that $SOD1^{mut}$ delays retro-translocation from ER lumen to the cytosol.

$SOD1^{mut}$ interacts specifically with Derlin-1

Since inhibition of the UPS is unlikely to be essential for $SOD1^{mut}$-induced ER stress (Fig. 1D; Supplemental Fig. S2A), disturbance of the retro-translocation system from the ER lumen to the cytoplasm may be a potential target of $SOD1^{mut}$. Various proteins involved in ERAD have been identified recently (Meusser et al. 2005). Among them, components of the retro-translocation machinery including ATPase p97, its cofactors Ufd1 and Npl4, and the ER membrane proteins Derlin-1 and VIMP are of key importance to ERAD function (Lilley and Ploegh 2004; Ye et al. 2004). We therefore examined the in vitro interactions of $SOD1^{mut}$ with p97, Ufd1, Npl4, VIMP, and Derlin-1. In vitro-translated ^{35}S-labeled Derlin-1, but not p97, Ufd1, Npl4, or VIMP, bound specifically to recombinant His-tagged $SOD1^{G93A}$ (Fig. 2A). To examine the interaction of Derlin-1 with different mutant forms of SOD1, several SOD1 mutants, including the A4V, G85R, and G93A mutants, were analyzed in mammalian cells. $SOD1^{A4V}$, $SOD1^{G85R}$, and $SOD1^{G93A}$, but not $SOD1^{wt}$, were clearly coimmunoprecipitated with Derlin-1 (Fig. 2B). The remaining ERAD components, including p97, Npl4, Ufd1, and VIMP, were not coimmunoprecipitated with $SOD1^{mut}$ (data not shown). The specific interaction between exogenous $SOD1^{mut}$ and endogenous Derlin-1 was also observed in NSC34 cells (Fig. 2C). These findings suggested that $SOD1^{mut}$ proteins specifically interact with Derlin-1 in mammalian cells.

To confirm these results in more physiological conditions, we examined the association of endogenous Derlin-1 and SOD1 in spinal cord of $SOD1^{G93A}$ gene transgenic ($SOD1^{G93A}$) mice. $SOD1^{G93A}$ mice showed the onset of motor function loss, which was measured using rota-rod test, at a mean age of 28.1 ± 1.3 wk, and died at a mean age of 34.9 ± 1.6 wk (see below and Fig. 5G). Accumulation of $SOD1^{mut}$ was observed in the spinal cord of $SOD1^{G93A}$ mice at the post-onset stage and the end stage (Fig. 2D). A strong interaction of endogenous Derlin-1 with exogenous $SOD1^{G93A}$, but not with exogenous $SOD1^{wt}$ (Supplemental Fig. S8A), was observed in parallel with accumulation of $SOD1^{mut}$ (Fig. 2D).

The reported expression pattern of Derlin-1 in mouse organs is controversial (Lilley and Ploegh 2005; Oda et al. 2006). We thus examined whether Derlin-1 is expressed in neuronal tissues of $SOD1^{wt}$ and $SOD1^{G93A}$ mice by immunoblotting analysis using a newly developed Derlin-1-specific antibody (Supplemental Fig. S4A). Derlin-1 proteins were clearly observed in many organs, including cerebral cortex, cerebellum, medulla, and spinal cord (Fig. 2E). Since human $SOD1^{G93A}$ gene is driven by human SOD1 promoter, $SOD1^{G93A}$ was widely expressed as expected in $SOD1^{G93A}$ mouse tissues (Fig. 2E; Epstein et al. 1987; Gurney et al. 1994). We also found that expression of $SOD1^{G93A}$ in neuronal tissues and liver was higher than that in other organs and that the interaction of Derlin-1 with $SOD1^{mut}$, but not $SOD1^{wt}$, was observed specifically in these tissues (Fig. 2E). The regionally specific interaction of Derlin-1 with $SOD1^{mut}$ might thus be one of the reasons why $SOD1^{mut}$ specifically targets neuronal tissues.

$SOD1^{mut}$ interacts with the C-terminal cytoplasmic region of Derlin-1

Although $SOD1^{mut}$ itself has neither a signal sequence nor transmembrane segment and is located mainly in the cytosol, it has been reported that $SOD1^{mut}$ accumulates in the ER (Kikuchi et al. 2006; Urushitani et al. 2006). We therefore examined whether $SOD1^{mut}$ resides in the ER lumen or associates with the cytosolic side of the ER membrane. Purified microsomal fraction enriched in the ER membrane was isolated from the spinal cord of a $SOD1^{G93A}$ mouse. We found that $SOD1^{G93A}$ exists mainly in the cytosolic fraction and some in the microsomal fraction (Fig. 2F). The alkaline extraction clearly released $SOD1^{G93A}$, but not Derlin-1, from the microsome, as seen for p97, which is known to be peripherally associated with the ER membrane (Fig. 2F). These findings indicated that $SOD1^{mut}$ exists mainly in the cytosol, and some fraction of $SOD1^{mut}$ attaches to the cytosolic surface of the ER.

Derlin-1 contains a domain named for yeast Der1p (Der1-like domain) and is a protein that spans the ER membrane four times, with both its N and C termini

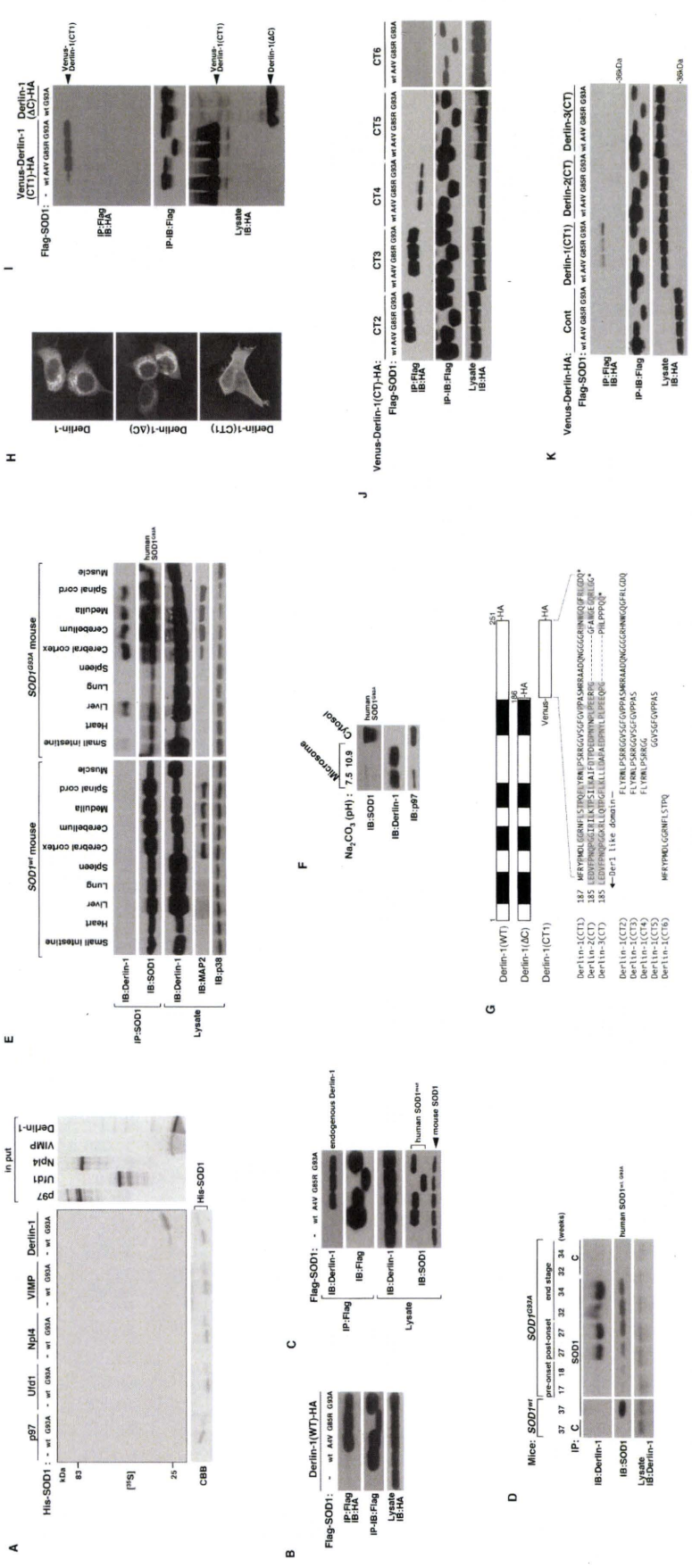

Figure 2. SOD1^{mut} interacts with Derlin-1. (*A*) ^{35}S-labeled p97, Ufd1, Npl4, VIMP, or Derlin-1 proteins were incubated with recombinant His-SOD1^{wt} or -SOD1^{G93A} proteins and immobilized on Ni-NTA beads (*top left*). The *bottom* part of the SDS-PAGE gel was stained with Coomassie brilliant blue dye (CBB). Amounts of incubated ^{35}S-labeled proteins are shown (input). (*B*) Lysates from HEK293 cells, transfected at the indicated combinations, were analyzed by IP-IB. (*C*) NSC34 cells were lysed after infection with Ad-Flag-SOD1^{wt}, Ad-Flag-SOD1^{A4V}, Ad-Flag-SOD1^{G85R}, or Ad-Flag-SOD1^{G93A} for 48 h and analyzed by IP-IB. (*D*) Extracts from spinal cords of mice were immunoprecipitated with an antibody to SOD1 (IP: SOD1) or control nonimmune antibody (IP: C) and analyzed by IB with antibodies to Derlin-1 and SOD1. The presence of Derlin-1 in the same lysates is shown. (*E*) Extracts from tissues of *SOD1*^{wt} mice and *SOD1*^{G93A} mice were analyzed by IB with antibodies to Derlin-1, MAP2, or p38. Interaction between SOD1^{mut} and Derlin-1 in tissues of *SOD1*^{G93A} mice was analyzed by IP-IB. (*F*) Spinal cord of *SOD1*^{G93A} mouse was homogenized and the microsomes were isolated from the post-nuclear and post-mitochondria homogenate. For alkaline extraction, the microsomes were incubated in 100 mM Na_2CO_3 (pH 7.5 or pH 10.9). After the incubation, the microsomes were pelleted and analyzed by IB with antibodies to Derlin-1, SOD1, and p97. Derlin-1 and p97 were used as controls for ER membrane-anchored protein and peripheral protein, respectively. (*G*) Schematic representation of various mutant forms of Derlin-1. Transmembrane domains of Derlin-1 are shown by black boxes. Identical residues of C-terminal fragment of Derlin family proteins are shaded. (*H*) HEK293 cells were transfected with various mutant forms of Derlin-1 and stained with antibody to HA. (*I–K*) Lysates from HEK293 cells, transfected at the indicated combinations, were analyzed by IP-IB.

facing the cytosol (Fig. 2G; Lilley and Ploegh 2004; Ye et al. 2004). To determine the domain of interaction, we constructed expression plasmids for a C-terminally truncated Derlin-1 protein [Derlin-1(ΔC)], which exhibited a reticular pattern, typical of ER localization, and for a C-terminal fragment of Derlin-1 [Derlin-1(CT1)], which exhibited cytosolic localization (Fig. 2H). Derlin-1(CT1), but not Derlin-1(ΔC), coimmunoprecipitated with $SOD1^{mut}$ (Fig. 2I), indicating that $SOD1^{mut}$ associates with the C-terminal cytosolic region of Derlin-1. To further investigate the region of interaction of Derlin-1(CT1) with $SOD1^{mut}$, various truncation mutants of the C-terminal fragment of Derlin-1 were assessed for interaction with $SOD1^{mut}$. Derlin-1(CT1), Derlin-1(CT2), Derlin-1(CT3), and Derlin-1(CT4), but not Derlin-1(CT5) and Derlin-1(CT6), were coimmunoprecipitated with $SOD1^{mut}$ (Fig. 2J), indicating that Derlin-1(CT4), composed of 12 amino acids (FLYRWLPSRRGG), is minimally required and sufficient for interaction with $SOD1^{mut}$. Mammals also express two additional Der1-like homologs to Derlin-1, designated Derlin-2 and Derlin-3 (Oda et al. 2006). To examine whether $SOD1^{mut}$ also interacts with other Derlin family proteins, C-terminal fragments of Derlin-2 and Derlin-3 [Derlin-2(CT) and Derlin-3(CT), respectively] were assessed for interaction with $SOD1^{mut}$. Derlin-2(CT) and Derlin-3(CT) were not coimmunoprecipitated with $SOD1^{mut}$ (Fig. 2K), suggesting that, among the Derlin family proteins, $SOD1^{mut}$ associates specifically with Derlin-1. Moreover, since mRNA expression of Derlin-1 was more abundant than that of Derlin-2 and Derlin-3 in brain (Oda et al. 2006), $SOD1^{mut}$ in neuronal tissues probably targets ERAD through specific binding to Derlin-1.

$SOD1^{mut}$ attenuates the retro-translocation of ERAD substrates on the components of ERAD machinery

There are at least three models for the mechanism of how ERAD is inhibited by $SOD1^{mut}$: (1) Since the C-terminal domain of Derlin-1 has been shown to be necessary for the recruitment of p97 on the ER membrane through binding with VIMP (Ye et al. 2004; Lilley and Ploegh 2005), $SOD1^{mut}$ might inhibit the assembly of Derlin-1, VIMP, and p97 on the ER membrane; (2) since Derlin-1 has been reported to form homo- as well as hetero-oligomers and the ERAD complex with HRD1, an ER-anchored ubiquitin E3 ligase (Lilley and Ploegh 2005; Schulze et al. 2005; Ye et al. 2005; Oda et al. 2006), $SOD1^{mut}$ might inhibit the interaction of Derlin-1 with these ERAD components; (3) $SOD1^{mut}$ might inhibit the directional flow of ERAD substrates at a certain step of their transfer from the ER lumen to p97 or E3 ligase. If the first two models were correct, overexpression of $SOD1^{mut}$ would inhibit the coimmunoprecipitation of Derlin-1 with VIMP, p97, or the other ERAD components. However, we could not detect any dissociation of VIMP (Fig. 3A), p97 (Fig. 3B), Derlin family proteins, and HRD1 (Fig. 3C) from Derlin-1 by $SOD1^{mut}$. To test model 3, we examined the interaction of an ERAD substrate (NHK) with Derlin-1. $SOD1^{mut}$, but not $SOD1^{wt}$, induced the interaction between NHK and Derlin-1 (Fig. 3D, top panel, lanes 2,6–8). Furthermore, NHK was found to associate with VIMP in the presence of Derlin-1 and $SOD1^{mut}$ (Fig. 3D, second panel, lanes 6–8), suggesting that $SOD1^{mut}$ induces formation of an NHK–Derlin-1–VIMP complex on the ER membrane.

The ERAD substrate that emerged into the cytosol is captured by p97, polyubiquitinated by E3 ligase, and degraded by the proteasome (Tsai et al. 2002; Meusser et al. 2005). We next examined whether $SOD1^{mut}$ inhibits ubiquitination of NHK. Overexpression of Derlin-1 increased the amount of ubiquitinated NHK in the presence of proteasome inhibitor (MG132) (Fig. 3E, top panel, lane 3), suggesting that Derlin-1 contributes to the degradation of NHK. Expression of $SOD1^{mut}$ clearly decreased the amount of ubiquitinated NHK (Fig. 3E, top panel, lanes 5–7). Furthermore, $SOD1^{mut}$ induced accumulation of nonubiquitinated and deglycosylated NHK in addition to glycosylated NHK (Fig. 3E, second panel, lanes 5–7), suggesting that $SOD1^{mut}$ blocks the presentation of NHK from retro-translocon to E3 ligase. These data also suggested that $SOD1^{mut}$ does not inhibit the assembly of essential components of retro-translocon per se but does trap ERAD substrates on the complex composed of $SOD1^{mut}$–Derlin-1–VIMP and thereby inhibits subsequent transfer of ERAD substrates to the ubiquitination step by E3.

$SOD1^{mut}$ activates the IRE1–TRAF2–ASK1 pathway

It has been reported that the ASK1–p38 pathway is activated in motor neurons of the spinal cord of $SOD1^{G93A}$ mice (Wengenack et al. 2004; Holasek et al. 2005; Veglianese et al. 2006). To investigate the role of ASK1 in the motor neurotoxicity by $SOD1^{mut}$, we examined whether $SOD1^{mut}$ activates ASK1 as assessed by in vitro kinase assay. Expression of $SOD1^{mut}$, but not $SOD1^{wt}$, activated endogenous ASK1 (Fig. 4A, top panel). We next examined whether $SOD1^{mut}$-induced ASK1 activation is mediated by ER stress. Activated IRE1 has been demonstrated to recruit TRAF2 and ASK1 on the ER membrane and thus to activate ASK1 (Nishitoh et al. 2002). We examined whether $SOD1^{mut}$ induces interaction between endogenous ASK1 and TRAF2. ASK1 was found to associate with TRAF2 in NSC34 cells infected with Ad-$SOD1^{mut}$ but not those infected with Ad-$SOD1^{wt}$ (Fig. 4A, third panel). To further examine whether IRE1 recruits TRAF2 and ASK1 in $SOD1^{mut}$-expressing cells, Ad-SOD1, Ad-ASK1, Ad-IRE1, and Lentivirus encoding (Len)-TRAF2 were infected into NSC34 cells and subjected to coimmunoprecipitation analysis. ASK1 was found to associate with IRE1 only in the presence of TRAF2 and $SOD1^{mut}$ (Fig. 4B), suggesting that $SOD1^{mut}$ induces formation of an IRE1–TRAF2–ASK1 complex on the ER membrane and thus activates ASK1 by triggering ER stress-induced IRE1 activation.

We next assessed the requirement of Derlin-1 for $SOD1^{mut}$-induced ER stress and ASK1 activation using siRNA against Derlin-1. Derlin-1 siRNA effectively sup-

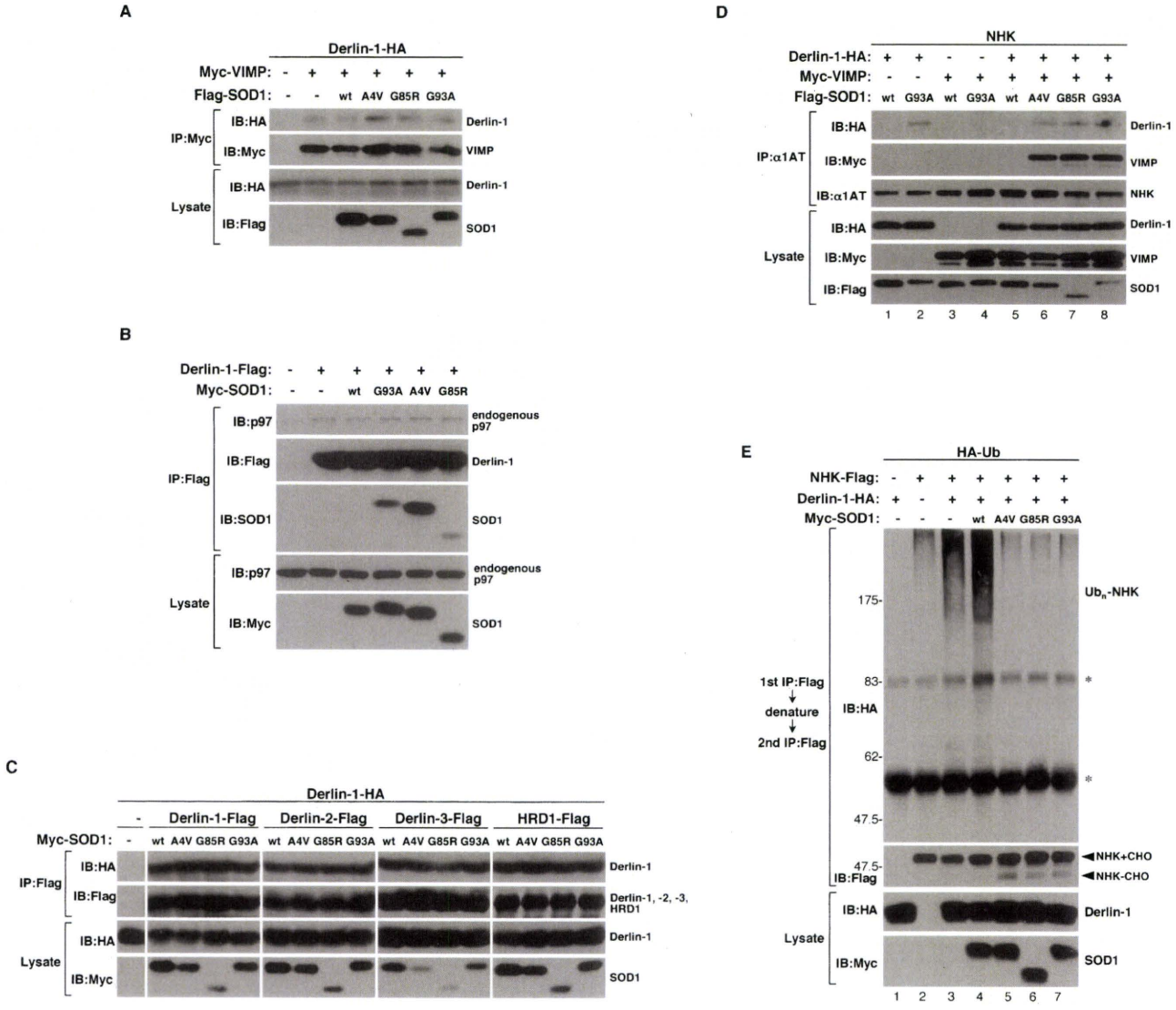

Figure 3. SOD1^{mut} attenuates the retro-translocation of ERAD substrate on the components of ERAD. (*A*) Lysates from HEK293 cells, transfected with Derlin-1-HA, Myc-VIMP, and Flag-SOD1 at the indicated combinations, were analyzed by IP-IB. The presence of Derlin-1-HA and Flag-SOD1 in the same lysates is shown. (*B*) Lysates from HEK293 cells, transfected at the indicated combinations, were analyzed by IP-IB. The presence of p97 and Myc-SOD1 in the same lysates is shown. (*C*) Lysates from HEK293 cells, transfected at the indicated combinations, were analyzed by IP-IB. The presence of Derlin-1-HA and Myc-SOD1 in the same lysates is shown. (*D*) Lysates from HEK293 cells, transfected with NHK, Derlin-1-HA, Myc-VIMP, and Flag-SOD1 at the indicated combinations, were analyzed by IP-IB. The presence of Derlin-1-HA, Myc-VIMP, and Flag-SOD1 in the same lysates is shown. (*E*) HEK293 cells were transfected with NHK-Flag, Derlin-1-HA, Myc-SOD1, and HA-Ub at the indicated combinations and incubated with 0.25 μM MG132 for 18 h. NHK was immunoprecipitated with antibody to Flag. After incubation with the denaturing buffer containing 1% SDS, NHK was reimmunoprecipitated with antibody to Flag. Samples were immunoblotted with antibodies to HA and Flag. The presence of Derlin-1-HA and Myc-SOD1 in the same lysates is shown. Asterisks denote nonspecific bands and IgG.

pressed expression of Derlin-1 without affecting that of Derlin-2, ASK1, p38, or TRAF2 (Fig. 4C,E). We examined whether reducing Derlin-1 expression levels affected the ER stress response using band-shift analyses of IRE1 and Xbp-1 mRNA splicing, which is caused by the activated RNase domain of IRE1. Derlin-1 siRNA exhibited no effect on the basal level of activation of IRE1 (Fig. 4C [lanes 1,5], D [lanes 1,7,13]) and thapsigargin-induced activation of IRE1 (Fig. 4C [lanes 4,8], D [lanes 6,12,18]), suggesting that Derlin-1 is not essential for ERAD in NSC34 cells. Interestingly, however, SOD1^{mut}-induced activation of IRE1 and ASK1 was clearly inhibited by Derlin-1 depletion (Fig. 4C [lane 7], D [lanes 9–11,15–17]). Furthermore, SOD1^{mut}-induced interaction between TRAF2 and ASK1 was inhibited by Derlin-1 depletion (Fig. 4E, lanes 9–11,15–17), suggesting that Derlin-1 is selectively required for the SOD1^{mut}-induced ER stress. These results also suggested that SOD1^{mut} induces ERAD dysfunction not by a simple loss of function but by a gain of malfunction of Derlin-1.

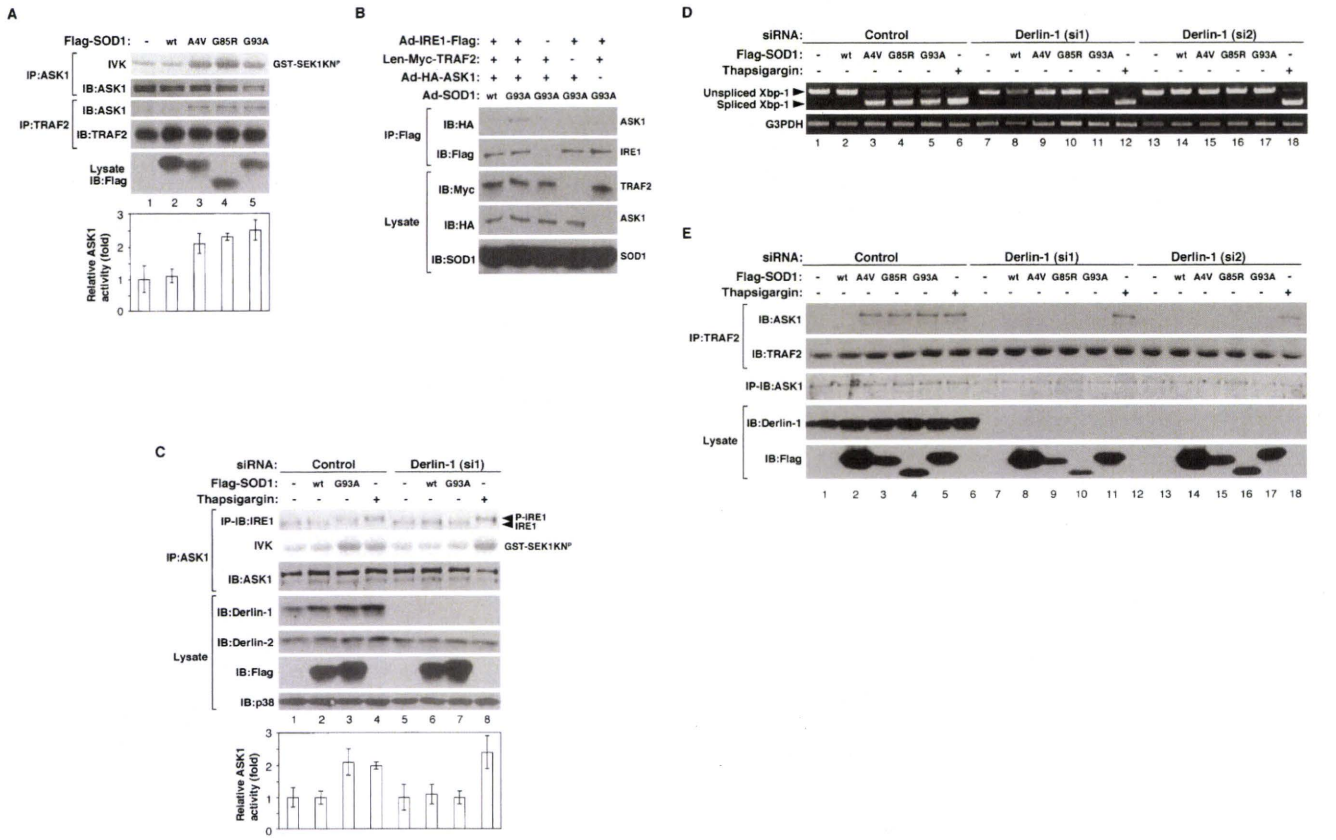

Figure 4. SOD1^{mut} activates the IRE1–TRAF2–ASK1 pathway. (*A*) NSC34 cells were infected with Ad-SOD1^{wt}, Ad-SOD1^{A4V}, Ad-SOD1^{G85R}, or Ad-SOD1^{G93A} for 48 h. ASK1 activity was measured by in vitro kinase assay (IVK). (GST-SEK1KN^{P}) Phosphorylated GST-SEK1KN. Interaction between TRAF2 and ASK1 was analyzed by IP with antibody to TRAF2 and IB with antibody to ASK1. The presence of ASK1, TRAF2, and SOD1 in the same lysates is shown. (Lane *1*) Kinase activity relative to the amount of ASK1 protein is shown as fold increase compared with control cells. (*B*) NSC34 cells were infected with adenoviruses and lentivirus at the indicated combinations. SOD1^{mut}-dependent IRE1–TRAF2–ASK1 complex formation were analyzed by IP-IB. (*C*) NSC34 cells, transfected with siRNA against Derlin-1 (si1) or nonspecific sequence (Control), were infected with Ad-SOD1^{wt} or Ad-SOD1^{G93A} for 48 h or treatment with 10 μM Thapsigargin for 2 h. Activation of IRE1 and ASK1 was analyzed by IP-IB with antibodies to IRE1α and by IVK using GST-SEK1KN as a substrate, respectively. The presence of ASK1, Derlin-1, Derlin-2, SOD1, and p38 in the same lysates is shown. (Lanes *1*,*5*) Kinase activity relative to the amount of ASK1 protein is shown as fold increase compared with control cells. (*D*,*E*) NSC34 cells, transfected with siRNA against Derlin-1 (si1), Derlin-1 (si2), or nonspecific sequence (Control), were infected with Ad-SOD1^{wt}, Ad-SOD1^{A4V}, Ad-SOD1^{G85R}, or Ad-SOD1^{G93A} for 48 h or treatment with 2 μM thapsigargin for 2 h. Xbp-1 mRNA splicing was determined by RT–PCR. Interaction between TRAF2 and ASK1 was analyzed by IP with antibody to TRAF2 and IB with antibody to ASK1. The presence of TRAF2, ASK1, Derlin-1, and Flag-SOD1 in the same lysates is shown.

Dissociation of SOD1^{mut} from Derlin-1 protects motor neurons from SOD1^{mut}-induced cell death

Based on the above findings, which indicate that SOD1^{mut} proteins induce ER stress by interacting with Derlin-1, we hypothesized that forced dissociation of SOD1^{mut} from Derlin-1 may restore normal function of ERAD and thus suppress SOD1^{mut}-induced motor neurotoxicity. We examined the effect of Derlin-1(CT4) on the interaction between SOD1^{mut} and Derlin-1. When Derlin-1(CT4) but not control (Venus-HA) or Derlin-1(CT5) was coexpressed, binding of Derlin-1 to SOD1^{mut} was strongly inhibited (Fig. 5A). Reciprocally, Derlin-1(CT4) was found to associate with SOD1^{mut} in a dose-dependent fashion (Fig. 5A). We next examined the effect of Derlin-1(CT4) on SOD1^{mut}-induced ER stress and ASK1 activation. Derlin-1(CT4) inhibited SOD1^{mut}-induced activation of IRE1, PERK, and ASK1 (Fig. 5B). These findings suggested that the interaction between SOD1^{mut} and Derlin-1 plays a central role in the activation of the ER stress–ASK1 pathway.

We next investigated the effects of Derlin-1(CT4) on SOD1^{mut}-induced cell death using spinal cord cultures derived from E12.5 mouse embryos (Urushitani et al. 2006). At 7 d after plating, spinal cord cultures were infected with Len-SOD1^{wt} or Len-SOD1^{mut} with Len-Derlin-1(CT4) or control (Venus-HA) lentivirus for additional 3 d. Expression of neither SOD1^{wt} nor SOD1^{G93A} affected the number of glial cells (Fig. 5C,F). In contrast, the number of motor neurons that were stained with antibody to unphosphorylated neurofilament-H (SMI32) was strongly decreased by SOD1^{G93A} (Fig. 5C,E) and SOD1^{G85R} (Supplemental Fig. S5A,B), indicating that SOD1^{mut} was selectively toxic to motor neurons and not

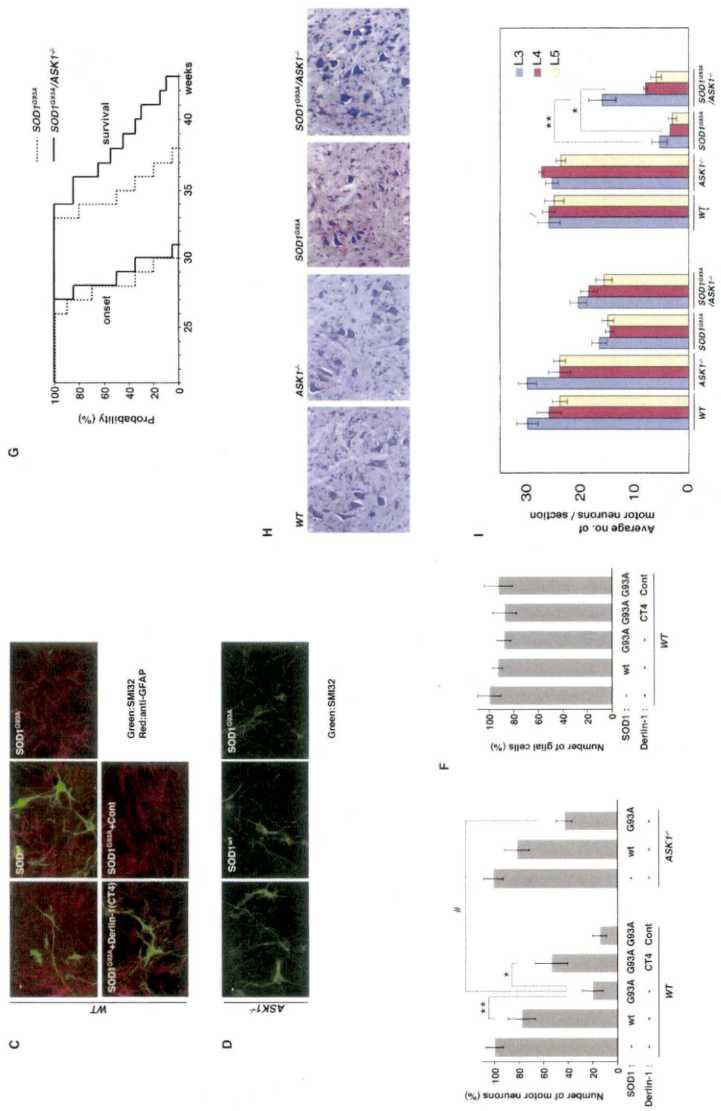

Figure 5. Impairment of SOD1^{mut}–Derlin-1 interaction and deletion of ASK1 mitigate SOD1^{mut}-induced motor neurotoxicity. (*A*) Lysates from HEK293 cells, transfected at the indicated combinations, were analyzed by IP-IB. (*B*) NSC34 cells were infected with Ad-SOD1^{wt}, Ad-SOD1^{G93A}, Len-Venus-Derlin-1(CT4)-HA, and Len-Venus-HA at the indicated combinations for 48 h. Activation of IRE1 and PERK was examined as described in Figure 1A. Activation of ASK1 was analyzed by IVK using GST-MKK6KN as substrate. (ASK1^{P}) Autophosphorylated ASK1. (GST-MKK6KN^{P}) Phosphorylated GST-MKK6KN. Asterisk denotes nonspecific bands. (*C*) Wild-type mice spinal cord cultures were infected with lentivirus at the indicated combinations for 72 h. Cultures were fixed and doubly stained with antibodies to nonphosphorylated neurofilament (SMI32) (green) and GFAP (red). (*D*) *ASK1*$^{-/-}$ mice spinal cord cultures were infected as indicated and stained with SMI32 antibody. (*E*) The percentage of total cell count of SMI32 antibody-positive cells is shown compared with control culture (wild type; $n = 3$); (*ASK1*$^{-/-}$; $n = 5$). Values are means ± SE of independent experiments. (*) $P < 0.05$; (**) $P < 0.01$; significance calculated by Student's *t*-test. (#) $P < 0.05$ significance calculated by ANOVA. (*F*) The percentage of total cell count of anti-GFAP antibody-positive cells derived from wild-type mice is shown compared with control culture. Values are means ± SE of three independent experiments. (*G*) The onset of disease was determined by motor function deficit seen in rota-rod performance in *SOD1*^{G93A} mice in the presence or absence (*ASK1*$^{-/-}$) of ASK1. The cumulative probability of onset of rota-rod deficit was not significantly changed in *SOD1*^{G93A}/*ASK1*$^{-/-}$ mice ($n = 10$; solid line) compared with *SOD1*^{G93A} mice ($n = 10$; dotted line). Probabilities of survival reveal prolongation of life span of *SOD1*^{G93A}/*ASK1*$^{-/-}$ mice ($n = 20$; solid line) compared with *SOD1*^{G93A} mice ($n = 20$; dotted line). The data were analyzed by the Kaplan-Meier life test and by long-rank test. (*H*) Cresyl violet (Nissl)-stained paraffin sections of ventral horn from lumbar (level L3) spinal cords at end stage (age 34 wk) are shown. (*I*) Stereological analysis of motor neuron death. Numbers of motor neurons were determined by counting the large Nissl-positive neurons in the ventral horn. Five mice of each group were used for analysis. Thirty-week-old and 34-wk-old mice were sacrificed, and sections of lumbar spinal cord at levels L3, L4, and L5 were counted for each mouse. Values are means ± SE. (*) $P < 0.05$; (**) $P < 0.01$; significance calculated by Student's *t*-test.

glial cells. SOD1^{mut}-induced motor neuron death was significantly attenuated by coexpression of Derlin-1(CT4) (Fig. 5C,E; Supplemental Fig. S5A,B). These findings are consistent with the inhibitory effects of Derlin-1(CT4) on the binding between SOD1^{mut} and Derlin-1 and on the ER stress-mediated activation of ASK1, and thus strongly suggested that induction of dysfunction of Derlin-1 by SOD1^{mut} may contribute to the pathogenesis of familial ALS.

ASK1 deficiency mitigates motor neuron death and prolongs survival of ALS mice

Finally, we examined the requirement of ASK1 for SOD1^{mut}-induced motor neuron death. Spinal cord cultures derived from wild-type and *ASK1*$^{-/-}$ mice were infected with Len-SOD1^{wt} or Len-SOD1^{G93A}. ASK1 deficiency did not affect the expression of SOD1^{wt} or SOD1^{G93A} (Supplemental Fig. S6). *ASK1*$^{-/-}$ neurons were significantly more resistant to SOD1^{mut}-induced cell death than were wild-type neurons (Fig. 5D,E). Inhibition of SOD1^{mut}-induced cell death in *ASK1*$^{-/-}$ neurons was not significantly enhanced by the expression of Derlin-1(CT4) (Supplemental Fig. S7), suggesting that the ASK1-dependent signal may serve as a major cell death pathway in the downstream SOD1^{mut}-induced ER stress. To further evaluate the role of ASK1 in the pathogenesis of ALS in vivo, we tested whether ASK1 deficiency ameliorates the motor neuropathological alterations in ALS mice. We produced *SOD1*^{G93A} mice that lacked *ASK1* (*SOD1*^{G93A}/*ASK1*$^{-/-}$ mice) (Supplemental Fig. S8B) and compared their time of disease onset and life span with those of *SOD1*^{G93A} mice. Time of disease onset was determined as that of loss of motor function. On rota-rod testing, no significant difference was found between *SOD1*^{G93A} and *SOD1*^{G93A}/*ASK1*$^{-/-}$ mice (Fig. 5G). However, the mean survival of *SOD1*^{G93A}/*ASK1*$^{-/-}$ mice was 38.4 ± 2.7 wk (±SEM) and significantly longer than the 34.9 ± 1.6 wk survival of control *SOD1*^{G93A} mice (long rank = 17.0206, $P < 0.0001$) (Fig. 5G). We also examined the time of disease onset and life span using *SOD1*^{G93A} high copy [*SOD1*$^{G93A(high)}$] mice. ASK1 deficiency also extended the survival of *SOD1*$^{G93A(high)}$ mice but not the time of onset (Supplemental Fig. S9). These findings indicated that ASK1 deficiency extends the survival of ALS mice by ameliorating disease progression. To assess the role of ASK1 in spinal motor neuron death in vivo, we examined L3, L4, and L5 spinal sections from wild-type, *ASK1*$^{-/-}$, *SOD1*^{G93A}, and *SOD1*^{G93A}/*ASK1*$^{-/-}$ mice. At the end stage, *SOD1*^{G93A} mice exhibited fewer motor neurons in the anterior horn of the spinal cord than age-matched wild-type or *ASK1*$^{-/-}$ mice (Fig. 5H; Supplemental Fig. S10A). In contrast, a larger number of motor neurons were significantly found in the upper (L3 and L4) spinal cord from *SOD1*^{G93A}/*ASK1*$^{-/-}$ than in that from *SOD1*^{G93A} mice (Fig. 5H,I; Supplemental Fig. S10A,B). These findings indicated that the absence of ASK1 mitigates motor neuron death in ALS mice.

Discussion

A novel pathogenic mechanism of SOD1^{mut}-mediated ALS is supported by the findings that SOD1^{mut} interacts specifically with Derlin-1 and that this interaction impairs ERAD and leads to ER stress-dependent activation of ASK1 (Fig. 6). The nearly complete loss of SOD1^{mut}-induced ER stress and activation of ASK1 by reduced expression of Derlin-1 or by overexpression of Derlin-1(CT4) strongly suggests that the binding between SOD1^{mut} and Derlin-1 is an important step in the SOD1^{mut}-induced ER stress signaling pathway. It has been reported that translocon-associated protein (TRAP) δ interacts with SOD1^{mut} (Kunst et al. 1997) and that TRAP complex including TRAPδ is required for ERAD (Nagasawa et al. 2007), suggesting that the association of SOD1^{mut} with TRAPδ may also be involved in SOD1^{mut}-induced ER stress.

It is unclear how various SOD1^{mut} proteins interact with Derlin-1. SOD1^{L126Z}, a simple C-terminal deletion mutant (Supplemental Fig. S11A), which causes motor neuron disease in mice (Wang et al. 2005), also interacted with Derlin-1 (Supplemental Fig. S11B). Therefore, the Derlin-1 interaction domain of SOD1^{wt} might be concealed by proper folding and be bared by mutation-dependent unfolding of SOD1^{mut}. Another hypothesis is that chaperon proteins might mediate the interaction between SOD1^{mut} and Derlin-1. Although the results from our in vitro studies using recombinant SOD1 proteins

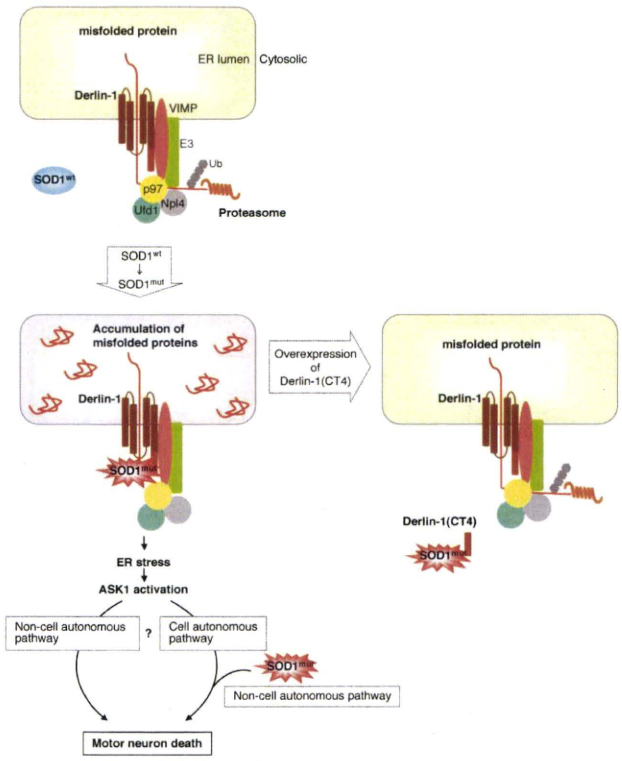

Figure 6. Schematic representation of the mechanism of SOD1^{mut}-induced motor neuron death through ER stress. See the text for details.

support a direct interaction between SOD1^{mut} and Derlin-1 (Fig. 2A), we cannot rule out the possibility that chaperon proteins in the reticulocyte lysate mediate the interaction between SOD1^{mut} and Derlin-1. SOD1^{mut}, but not SOD1^{wt}, is known to interact with heat shock proteins, including Hsp25 and Hsp/Hsc70 (Shinder et al. 2001; Wang et al. 2003; Urushitani et al. 2004).

It is still unclear how the association of SOD1^{mut} with Derlin-1 inhibits the ERAD pathway. Derlin-1 is one of the components required for retro-translocation of misfolded proteins from the ER lumen to the cytoplasm (Lilley and Ploegh 2004; Ye et al. 2004). Derlin-1-mediated retro-translocation is currently believed to occur as follows (Meusser et al. 2005): (1) The substrate is recognized by ER chaperones or ER membrane receptors and is targeted to a retro-translocon; (2) Derlin-1 recruits a membrane complex containing VIMP, the p97 complex, and an E3 ligase; (3) once the substrate emerges into the cytosol, it is captured by p97 as a result of its AAA-ATPase activity and polyubiquitinated by E3; and (4) subsequently, the polyubiquitinated substrates are degraded by the proteasome. The present finding that inhibition of proteasomal activity was undetectable by SOD1^{mut} at the time at which SOD1^{mut}-induced ER stress was evoked (Fig. 1D; Supplemental Fig. S2A) suggests that it is unlikely that SOD1^{mut} primarily targeted final step 4. If SOD1^{mut} disturbs the initiation step 1 of retro-translocation, SOD1^{mut} may inhibit interaction between the unfolded substrate and Derlin-1. However, binding between NHK and Derlin-1 was clearly observed even in SOD1^{mut}-overexpressing cells (Fig. 3D). Moreover, SOD1^{mut} did not inhibit association of Derlin-1 with VIMP, p97, Derlin family proteins, and HRD1 (Fig. 3A–C), suggesting that SOD1^{mut} may not perturb step 2. However, we cannot rule out the possibility that SOD1^{mut} inhibits additional interactions between Derlin-1 and its partners in the ERAD complex. Since ubiquitination of ERAD substrate was inhibited by SOD1^{mut} (Fig. 3E), SOD1^{mut} may thus disturb the presentation of ERAD substrate to the p97 complex or E3. Although exactly how SOD1^{mut} inhibits the directional flow of ERAD substrates remains to be elucidated, it is imaginable that ERAD substrates trapped on the SOD1^{mut}–Derlin-1–VIMP complex would interfere with further disposal of de novo ERAD substrates like a traffic jam, eventually leading to the accumulation of misfolded proteins within the ER lumen.

Although the prolongation of survival of *SOD1^{G93A}/ASK1$^{-/-}$* mice clearly indicated the requirement of ASK1 for disease progression, ASK1 deficiency was not sufficient to attenuate disease onset (Fig. 5G; Supplemental Fig. S9). These findings are supported by a recent study that demonstrated the contribution of caspase-9 to motor neuron death and disease progression but not to disease onset in *X-chromosome-linked inhibitor of apoptosis* (*XIAP*; a mammalian inhibitor of caspase-3 and caspase-9) transgenic mice (Inoue et al. 2003). We reported previously that ASK1-induced apoptosis is dependent on caspase-9 activation (Hatai et al. 2000), suggesting that the ASK1–caspase-9 proapoptotic pathway may be crucial only for disease progression. On the other hand, several groups have reported that the p38, but not JNK, pathway is activated in motor neurons of the spinal cord of *SOD1^{G93A}* mice (Wengenack et al. 2004; Holasek et al. 2005; Veglianese et al. 2006). Thus, the ASK1–p38 and/or ASK1–caspase-9 pathway may specifically contribute to SOD1^{mut}-induced motor neuron death.

Since expression of Derlin-1(CT4) and deletion of ASK1 only partially mitigated SOD1^{mut}-induced motor neuron death in vitro (Fig. 5E; Supplemental Fig. S5B), the ER stress–ASK1 pathway-independent cell death mechanism including proteasomal dysfunction (Urushitani et al. 2002; Puttaparthi et al. 2003) may also exist in the pathogenesis of ALS. This may reflect, in part, the incomplete resistance of motor neuron death by ASK1 deficiency in ALS mice (Fig. 5I; Supplemental Fig. S10B). Furthermore, the effect of loss of ASK1 on cell death was slightly weaker than that of Derlin-1(CT4) (Fig. 5E), and Derlin-1(CT4) slightly, although not significantly, enhanced the inhibition of SOD1^{mut}-induced cell death in *ASK1$^{-/-}$* neurons (Supplemental Fig. S7). These results suggest that other ER stress-induced proapoptotic pathways, including PERK (Jordan et al. 2002) and CHOP (Zinszner et al. 1998), might also be involved in the downstream SOD1^{mut}-dependent motor neuron death.

Another important issue to be elucidated is the relationship between the ER stress-mediated signaling pathway and the non-cell-autonomous mechanisms of SOD1^{mut}-induced neurotoxicity. Recent studies have emphasized the importance of non-cell-autonomous mechanisms (Clement et al. 2003; Boillee et al. 2006; Yamanaka et al. 2008). Consistent with their findings, SOD1^{mut} induced motor neuron death in spinal cord cultures (Fig. 5C,E; Supplemental Fig. S5A,B) but not in NSC34 cells (data not shown) in which ER stress-mediated ASK1 activation was clearly observed. However, since expression of SOD1^{mut} in neurons alone (Pramatarova et al. 2001) or glial cells alone (Gong et al. 2000) does not induce motor neuron disease in mice, not only non-cell-autonomous mechanisms but also cell-autonomous mechanisms must play roles in SOD1^{mut}-induced neurotoxicity. It is likely that the non-cell-autonomous signals that are transferred from astrocytes, glial cells, or feeder cells to motor neurons are coordinated with and crucial for the ER stress/ASK1-dependent cell-autonomous death signaling induced by SOD1^{mut} (Fig. 6). It is also possible that the ER stress-induced ASK1 activation itself serves as the non-cell-autonomous death signaling (Fig. 6).

In conclusion, our findings demonstrated a novel mechanism by which SOD1^{mut} causes motor neuron death through interaction with Derlin-1, ERAD dysfunction, ER stress, and ASK1 activation. Although further investigation is needed to clarify the mechanisms by which SOD1^{mut} induces the malfunction of Derlin-1 and to identify the downstream effectors of ASK1, Derlin-1 and ASK1 may be potential targets in the treatment of ALS.

Materials and methods

Band-shift analysis for IRE1 and PERK

NSC34 cells were lysed in the lysis buffer as described (Nishitoh et al. 2002). Cell extracts were clarified by centrifugation, and the supernatants were immunoprecipitated with antibodies to IRE1α and PERK. Proteins were resolved by SDS-PAGE under reducing conditions and immunoblotted with antibodies to IRE1α and PERK.

RT–PCR

Total RNA was isolated from 6×10^5 NSC34 cells using ISOGEN kit (Nippongene). Ten micrograms of RNA were reverse-transcribed with SuperScript II (Life Technologies) according to the manufacturer's instructions. The primers used for PCR were as follows: mouse BiP, 5′-AAGGTCTATGAAGGTGAACGACCCC-3′ and 5′-GACCCCAAGACATGTGAGCAACTGC-3′; mouse CHOP, 5′-ACTACTCTTGACCCTGCGTCCCTAG-3′ and 5′-CATGTGCAGTGCAGTGCAGGGTCAC-3′; mouse Xbp-1, 5′-GAACCAGGAGTTAAGAACACG-3′ and 5′-AGGCAACAGTGTCAGAGTCC-3′; and mouse G3PDH, 5′-ATGGTGAAGGTCGGTGTGAA-3′ and 5′-ACATGGCCTCCAAGGAGTAA-3′.

Pulse-chase assay

NSC cells were labeled with ^{35}S-Promix (GE Healthcare) in medium lacking methionine and cystein for 30 min, and chased in medium containing excess methionine and cystein. Cells were lysed in a buffer containing 1% NP-40, 150 mM NaCl, 50 mM Tris-HCl (pH 8.0), and protease inhibitor cocktail. An antibody to α1AT was used for immunoprecipitation. Immunoprecipitated samples were resolved by SDS-PAGE and analyzed by an image analyzer.

In vitro binding assay

His^6-SOD1^{wt} and His^6-SOD1^{G93A} were constructed in pTrcHis vector (Invitrogen). Recombinant His-SOD1^{wt} and His-SOD1^{G93A} proteins were purified with Ni-NTA (Qiagen) according to the manufacturer's instructions. In vitro translated ^{35}S-labeled VCP, Ufd1, Npl4, VIMP, and Derlin-1 were prepared with the TNT Reticulocyte Lysate System (Promega). ^{35}S-labeled proteins were incubated for 16 h at 4°C with each His-SOD1^{WT} or His-SOD1^{G93A} in buffer containing 150 mM NaCl, 20 mM Tris-HCl (pH 7.5), and 0.5 mM Triton X-100; washed twice with the washing buffer containing 150 mM NaCl, 20 mM Tris-HCl (pH 7.5), 0.5% Triton X-100, and 20 mM Imidazole; and analyzed by SDS-PAGE with an image analyzer.

In vivo binding assay

Binding assay using transfected HEK293 cells has been described (Nishitoh et al. 2002). For binding assay between overexpressed Flag-SOD1 and endogenous Derlin-1, ~5×10^6 NSC34 cells infected with Ad-SOD1^{wt}, Ad-SOD1^{A4V}, Ad-SOD1^{G85R}, or Ad-SOD1^{G93A} for 48 h were immunoprecipitated with an antibody to Flag. For endogenous binding assay between SOD1 and Derlin-1, lysates from tissues of *SOD1^{wt}* or *SOD1^{G93A}* mice were immunoprecipitated with an antibody to SOD1 or control nonimmune rabbit polyclonal antibody. For endogenous binding assay between TRAF2 and ASK1, lysates from ~3×10^7 NSC34 cells were immunoprecipitated with an antibody to TRAF2 or control nonimmune rabbit polyclonal antibody. Proteins were resolved by SDS-PAGE and immunoblotted with antibodies to Derlin-1, SOD1, ASK1, or TRAF2. Aliquots of the same lysates were subjected to immunoblotting with antibodies to Derlin-1 or Flag. For the complex formation assay of IRE1–TRAF2–ASK1, ~1×10^7 NSC34 cells were infected with adenoviruses and lentivirus for 48 h, and lysates were analyzed by immunoprecipitation-immunoblot (IP-IB) as described (Nishitoh et al. 2002).

Subcellular fractionation

A 30-wk-old mouse spinal cord was washed with PBS at 4°C and placed in ice-cold homogenization buffer (10 mM Tris-HCl at pH 7.4, 1 mM EDTA, protease inhibitors). Tissue was homogenized with 40 strokes of a glass-pestle homogenizer on ice. Homogenates were centrifuged at 14,000*g* for 7 min. Supernatant was centrifuged at 100,000*g* for 1 h to yield a microsomal pellet. Microsomes were incubated with homogenization buffer containing 100 mM Na_2CO_3 (pH 7.5 or pH 10.9) for 5 min, pelleted by centrifugation at 100,000*g* for 30 min, and analyzed by IB with an antibody to SOD1, Derlin-1, or p97.

In vitro kinase assay

In vitro kinase assay has been described (Nishitoh et al. 2002). In brief, infected 1×10^7 NSC34 cells were lysed with the lysis buffer and immunoprecipitated with an antibody to ASK1. Kinase activity of ASK1 was measured using [γ-^{32}P]ATP and GST-MKK6KN or GST-SEK1KN as substrate and analyzed by SDS-PAGE with an image analyzer.

Ubiquitination assay

Lysates from transfected HEK293 cells were immunoprecipitated with antibody to Flag. After washing with the washing buffer containing 150 mM NaCl, 20 mM Tris-HCl (pH 7.5), and 5 mM EGTA, beads were boiled with the denaturing buffer containing 1% SDS, 150 mM NaCl, 20 mM Tris-HCl (pH 7.5), and 5 mM EGTA. The supernatant was diluted and reimmunoprecipitated with antibody to Flag and analyzed by SDS-PAGE.

siRNA knockdown of Derlin-1

NSC34 cells were transfected with Derlin-1-specific RNAi oligo and control RNAi oligo (Invitrogen) using Lipofectamine RNAiMAX reagent (Invitrogen). After 24 h, cells were infected with adenovirus for 48 h. Knockdown was analyzed by IB with antibody to Derlin-1. Sequences were as follows: Derl1-MSS228692 (si1) Stealth Select RNAi, AUAUAGUUGAAUCCAAGGAUAACCC and GGGUUAUCCUUGGAUUCAACUAUAU; Derl1-MSS228693 (si2) Stealth Select RNAi, AGUAACAGGCCUUAAAUCGCGUUCC and GGAACGCGAUUUAAGGCCUGUUACU; and Stealth RNAi Negative Control Medium GC Duplex.

Motor neuron death assay

Spinal cords (Urushitani et al. 2002) were subjected to primary culture for 7 d and infected with lentivirus for 72 h. Cells were stained with antibody to GFAP (1:100; DAKO) and SMI32 antibody (1:1000; Covance).

Mice

Both $SOD1^{G93A}$ transgenic mice (G1L/+ line, backcrossed to C57BL/6 mice; Jackson Laboratories), which expressed human $SOD1^{G93A}$ gene, and $SOD1^{wt}$ transgenic mice, which expressed >8 copies of human $SOD1^{wt}$ gene, were used. An $ASK1^{-/-}$ mouse (Tobiume et al. 2001) was mated with a $SOD1^{G93A}$ mouse under pathogen-free conditions. To circumvent potential difficulties caused by sex of mice, male mice were utilized in the present study. The onset of disease was determined by motor function deficit seen in rota-rod performance at an accelerated speed to 40 rpm for 5 min. All mouse experiments accorded with protocols approved by the Animal Research Committees of Tokyo Medical and Dental University and the University of Tokyo.

Nissl staining

Mice were perfused with PBS followed by 4% PFA in PBS. The spinal cords were excised, fixed with 4% PFA in PBS for 1 d, embedded in paraffin, and sectioned (4 μm). After being deparaffinized using standard protocols, paraffin sections were nissl-stained with cresyl violet. All motor neuron counts were performed in a blinded fashion. We counted the numbers of motor neurons in every fifth section of L3, L4, and L5. Only the large-size neurons with a clear nucleolus and distinctly labeled cytoplasm were included in cell counts.

Acknowledgments

We thank R. Takahashi and M. Urushitani for kind instruction for the primary motor neuron culture; D. Ron, F. Urano, T.A. Rapoport, and Y. Ye for providing antibodies; K. Nagata and N. Hosokawa for providing NHK plasmid; and D. Trono for providing the lentiviral vector system. We also thank all the members of Cell Signaling Laboratory for their critical comments. This study was supported by Grant-in-Aid for Scientific Research on Priority Areas, Research on Pathomechanisms of Brain Disorders, from the Ministry of Education, Culture, Sports, Science and Technology of Japan, CREST, Japan Science and Technology Corporation, Takeda Science Foundation, and The Nakabayashi Trust for ALS Research.

References

Atkin, J.D., Farg, M.A., Turner, B.J., Tomas, D., Lysaght, J.A., Nunan, J., Rembach, A., Nagley, P., Beart, P.M., Cheema, S.S., et al. 2006. Induction of the unfolded protein response in familial amyotrophic lateral sclerosis and association of protein disulfide isomerase with superoxide dismutase 1. *J. Biol. Chem.* **281:** 30152–30165.

Boillee, S., Yamanaka, K., Lobsiger, C.S., Copeland, N.G., Jenkins, N.A., Kassiotis, G., Kollias, G., and Cleveland, D.W. 2006. Onset and progression in inherited ALS determined by motor neurons and microglia. *Science* **312:** 1389–1392.

Bowling, A.C., Schulz, J.B., Brown Jr., R.H., and Beal, M.F. 1993. Superoxide dismutase activity, oxidative damage, and mitochondrial energy metabolism in familial and sporadic amyotrophic lateral sclerosis. *J. Neurochem.* **61:** 2322–2325.

Clement, A.M., Nguyen, M.D., Roberts, E.A., Garcia, M.L., Boillee, S., Rule, M., McMahon, A.P., Doucette, W., Siwek, D., Ferrante, R.J., et al. 2003. Wild-type nonneuronal cells extend survival of SOD1 mutant motor neurons in ALS mice. *Science* **302:** 113–117.

Epstein, C.J., Avraham, K.B., Lovett, M., Smith, S., Elroy-Stein, O., Rotman, G., Bry, C., and Groner, Y. 1987. Transgenic mice with increased Cu/Zn-superoxide dismutase activity: Animal model of dosage effects in Down syndrome. *Proc. Natl. Acad. Sci.* **84:** 8044–8048.

Fang, S., Ferrone, M., Yang, C., Jensen, J.P., Tiwari, S., and Weissman, A.M. 2001. The tumor autocrine motility factor receptor, gp78, is a ubiquitin protein ligase implicated in degradation from the endoplasmic reticulum. *Proc. Natl. Acad. Sci.* **98:** 14422–14427.

Gong, Y.H., Parsadanian, A.S., Andreeva, A., Snider, W.D., and Elliott, J.L. 2000. Restricted expression of G86R Cu/Zn superoxide dismutase in astrocytes results in astrocytosis but does not cause motoneuron degeneration. *J. Neurosci.* **20:** 660–665.

Gurney, M.E., Pu, H., Chiu, A.Y., Dal Canto, M.C., Polchow, C.Y., Alexander, D.D., Caliendo, J., Hentati, A., Kwon, Y.W., Deng, H.X., et al. 1994. Motor neuron degeneration in mice that express a human Cu,Zn superoxide dismutase mutation. *Science* **264:** 1772–1775.

Hatai, T., Matsuzawa, A., Inoshita, S., Mochida, Y., Kuroda, T., Sakamaki, K., Kuida, K., Yonehara, S., Ichijo, H., and Takeda, K. 2000. Execution of apoptosis signal-regulating kinase 1 (ASK1)-induced apoptosis by the mitochondria-dependent caspase activation. *J. Biol. Chem.* **275:** 26576–26581.

Holasek, S.S., Wengenack, T.M., Kandimalla, K.K., Montano, C., Gregor, D.M., Curran, G.L., and Poduslo, J.F. 2005. Activation of the stress-activated MAP kinase, p38, but not JNK in cortical motor neurons during early presymptomatic stages of amyotrophic lateral sclerosis in transgenic mice. *Brain Res.* **1045:** 185–198.

Inoue, H., Tsukita, K., Iwasato, T., Suzuki, Y., Tomioka, M., Tateno, M., Nagao, M., Kawata, A., Saido, T.C., Miura, M., et al. 2003. The crucial role of caspase-9 in the disease progression of a transgenic ALS mouse model. *EMBO J.* **22:** 6665–6674.

Jordan, R., Wang, L., Graczyk, T.M., Block, T.M., and Romano, P.R. 2002. Replication of a cytopathic strain of bovine viral diarrhea virus activates PERK and induces endoplasmic reticulum stress-mediated apoptosis of MDBK cells. *J. Virol.* **76:** 9588–9599.

Julien, J.P. and Beaulieu, J.M. 2000. Cytoskeletal abnormalities in amyotrophic lateral sclerosis: Beneficial or detrimental effects? *J. Neurol. Sci.* **180:** 7–14.

Kikuchi, H., Almer, G., Yamashita, S., Guegan, C., Nagai, M., Xu, Z., Sosunov, A.A., McKhann, G.M.I., and Przedborski, S. 2006. Spinal cord endoplasmic reticulum stress associated with a microsomal accumulation of mutant superoxide dismutase-1 in an ALS model. *Proc. Natl. Acad. Sci.* **103:** 6025–6030.

Kirby, J., Halligan, E., Baptista, M.J., Allen, S., Heath, P.R., Holden, H., Barber, S.C., Loynes, C.A., Wood-Allum, C.A., Lunec, J., et al. 2005. Mutant SOD1 alters the motor neuronal transcriptome: Implications for familial ALS. *Brain* **128:** 1686–1706.

Kopito, R.R. 1997. ER quality control: The cytoplasmic connection. *Cell* **88:** 427–430.

Kunst, C.B., Mezey, E., Brownstein, M.J., and Patterson, D. 1997. Mutations in SOD1 associated with amyotrophic lateral sclerosis cause novel protein interactions. *Nat. Genet.* **15:** 91–94.

Li, M., Ona, V.O., Guegan, C., Chen, M., Jackson-Lewis, V., Andrews, L.J., Olszewski, A.J., Stieg, P.E., Lee, J.P., Przedborski, S., et al. 2000. Functional role of caspase-1 and caspase-3 in an ALS transgenic mouse model. *Science* **288:** 335–339.

Lilley, B.N. and Ploegh, H.L. 2004. A membrane protein required for dislocation of misfolded proteins from the ER. *Nature* **429:** 834–840.

Lilley, B.N. and Ploegh, H.L. 2005. Multiprotein complexes that link dislocation, ubiquitination, and extraction of misfolded proteins from the endoplasmic reticulum membrane. *Proc. Natl. Acad. Sci.* **102:** 14296–14301.

Liu, J., Lillo, C., Jonsson, P.A., Vande Velde, C., Ward, C.M., Miller, T.M., Subramaniam, J.R., Rothstein, J.D., Marklund, S., Andersen, P.M., et al. 2004. Toxicity of familial ALS-linked SOD1 mutants from selective recruitment to spinal mitochondria. *Neuron* **43:** 5–17.

Meusser, B., Hirsch, C., Jarosch, E., and Sommer, T. 2005. ERAD: The long road to destruction. *Nat. Cell Biol.* **7:** 766–772.

Nagasawa, K., Higashi, T., Hosokawa, N., Kaufman, R.J., and Nagata, K. 2007. Simultaneous induction of the four subunits of the TRAP complex by ER stress accelerates ER degradation. *EMBO Rep.* **8:** 483–489.

Nishitoh, H., Matsuzawa, A., Tobiume, K., Saegusa, K., Takeda, K., Inoue, K., Hori, S., Kakizuka, A., and Ichijo, H. 2002. ASK1 is essential for endoplasmic reticulum stress-induced neuronal cell death triggered by expanded polyglutamine repeats. *Genes & Dev.* **16:** 1345–1355.

Oda, Y., Okada, T., Yoshida, H., Kaufman, R.J., Nagata, K., and Mori, K. 2006. Derlin-2 and Derlin-3 are regulated by the mammalian unfolded protein response and are required for ER-associated degradation. *J. Cell Biol.* **172:** 383–393.

Pasinelli, P., Borchelt, D.R., Houseweart, M.K., Cleveland, D.W., and Brown Jr., R.H. 1998. Caspase-1 is activated in neural cells and tissue with amyotrophic lateral sclerosis-associated mutations in copper–zinc superoxide dismutase. *Proc. Natl. Acad. Sci.* **95:** 15763–15768.

Pramatarova, A., Laganiere, J., Roussel, J., Brisebois, K., and Rouleau, G.A. 2001. Neuron-specific expression of mutant superoxide dismutase 1 in transgenic mice does not lead to motor impairment. *J. Neurosci.* **21:** 3369–3374.

Puttaparthi, K., Wojcik, C., Rajendran, B., DeMartino, G.N., and Elliott, J.L. 2003. Aggregate formation in the spinal cord of mutant SOD1 transgenic mice is reversible and mediated by proteasomes. *J. Neurochem.* **87:** 851–860.

Raoul, C., Estevez, A.G., Nishimune, H., Cleveland, D.W., deLapeyriere, O., Henderson, C.E., Haase, G., and Pettmann, B. 2002. Motoneuron death triggered by a specific pathway downstream of Fas. potentiation by ALS-linked SOD1 mutations. *Neuron* **35:** 1067–1083.

Schulze, A., Standera, S., Buerger, E., Kikkert, M., van Voorden, S., Wiertz, E., Koning, F., Kloetzel, P.M., and Seeger, M. 2005. The ubiquitin-domain protein HERP forms a complex with components of the endoplasmic reticulum associated degradation pathway. *J. Mol. Biol.* **354:** 1021–1027.

Sekine, Y., Takeda, K., and Ichijo, H. 2006. The ASK1–MAP kinase signaling in ER stress and neurodegenerative diseases. *Curr. Mol. Med.* **6:** 87–97.

Shinder, G.A., Lacourse, M.C., Minotti, S., and Durham, H.D. 2001. Mutant Cu/Zn-superoxide dismutase proteins have altered solubility and interact with heat shock/stress proteins in models of amyotrophic lateral sclerosis. *J. Biol. Chem.* **276:** 12791–12796.

Sifers, R.N., Brashears-Macatee, S., Kidd, V.J., Muensch, H., and Woo, S.L. 1988. A frameshift mutation results in a truncated α 1-antitrypsin that is retained within the rough endoplasmic reticulum. *J. Biol. Chem.* **263:** 7330–7335.

Suzuki, T., Park, H., and Lennarz, W.J. 2002. Cytoplasmic peptide:N-glycanase (PNGase) in eukaryotic cells: Occurrence, primary structure, and potential functions. *FASEB J.* **16:** 635–641.

Tobisawa, S., Hozumi, Y., Arawaka, S., Koyama, S., Wada, M., Nagai, M., Aoki, M., Itoyama, Y., Goto, K., and Kato, T. 2003. Mutant SOD1 linked to familial amyotrophic lateral sclerosis, but not wild-type SOD1, induces ER stress in COS7 cells and transgenic mice. *Biochem. Biophys. Res. Commun.* **303:** 496–503.

Tobiume, K., Matsuzawa, A., Takahashi, T., Nishitoh, H., Morita, K., Takeda, K., Minowa, O., Miyazono, K., Noda, T., and Ichijo, H. 2001. ASK1 is required for sustained activations of JNK/p38 MAP kinases and apoptosis. *EMBO Rep.* **2:** 222–228.

Tsai, B., Ye, Y., and Rapoport, T.A. 2002. Retro-translocation of proteins from the endoplasmic reticulum into the cytosol. *Nat. Rev. Mol. Cell Biol.* **3:** 246–255.

Urushitani, M., Kurisu, J., Tsukita, K., and Takahashi, R. 2002. Proteasomal inhibition by misfolded mutant superoxide dismutase 1 induces selective motor neuron death in familial amyotrophic lateral sclerosis. *J. Neurochem.* **83:** 1030–1042.

Urushitani, M., Kurisu, J., Tateno, M., Hatakeyama, S., Nakayama, K., Kato, S., and Takahashi, R. 2004. CHIP promotes proteasomal degradation of familial ALS-linked mutant SOD1 by ubiquitinating Hsp/Hsc70. *J. Neurochem.* **90:** 231–244.

Urushitani, M., Sik, A., Sakurai, T., Nukina, N., Takahashi, R., and Julien, J.P. 2006. Chromogranin-mediated secretion of mutant superoxide dismutase proteins linked to amyotrophic lateral sclerosis. *Nat. Neurosci.* **9:** 108–118.

Veglianese, P., Lo Coco, D., Bao Cutrona, M., Magnoni, R., Pennacchini, D., Pozzi, B., Gowing, G., Julien, J.P., Tortarolo, M., and Bendotti, C. 2006. Activation of the p38MAPK cascade is associated with upregulation of TNF α receptors in the spinal motor neurons of mouse models of familial ALS. *Mol. Cell. Neurosci.* **31:** 218–231.

Wang, J., Slunt, H., Gonzales, V., Fromholt, D., Coonfield, M., Copeland, N.G., Jenkins, N.A., and Borchelt, D.R. 2003. Copper-binding-site-null SOD1 causes ALS in transgenic mice: Aggregates of non-native SOD1 delineate a common feature. *Hum. Mol. Genet.* **12:** 2753–2764.

Wang, J., Xu, G., Li, H., Gonzales, V., Fromholt, D., Karch, C., Copeland, N.G., Jenkins, N.A., and Borchelt, D.R. 2005. Somatodendritic accumulation of misfolded SOD1-L126Z in motor neurons mediates degeneration: αB-crystallin modulates aggregation. *Hum. Mol. Genet.* **14:** 2335–2347.

Wengenack, T.M., Holasek, S.S., Montano, C.M., Gregor, D., Curran, G.L., and Poduslo, J.F. 2004. Activation of programmed cell death markers in ventral horn motor neurons during early presymptomatic stages of amyotrophic lateral sclerosis in a transgenic mouse model. *Brain Res.* **1027:** 73–86.

Wong, P.C., Pardo, C.A., Borchelt, D.R., Lee, M.K., Copeland, N.G., Jenkins, N.A., Sisodia, S.S., Cleveland, D.W., and Price, D.L. 1995. An adverse property of a familial ALS-linked SOD1 mutation causes motor neuron disease characterized by vacuolar degeneration of mitochondria. *Neuron* **14:** 1105–1116.

Yamanaka, K., Chun, S.J., Boillee, S., Fujimori-Tonou, N., Yamashita, H., Gutmann, D.H., Takahashi, R., Misawa, H., and Cleveland, D.W. 2008. Astrocytes as determinants of disease progression in inherited amyotrophic lateral sclerosis. *Nat. Neurosci.* **11:** 251–253.

Ye, Y., Shibata, Y., Yun, C., Ron, D., and Rapoport, T.A. 2004. A membrane protein complex mediates retro-translocation from the ER lumen into the cytosol. *Nature* **429:** 841–847.

Ye, Y., Shibata, Y., Kikkert, M., van Voorden, S., Wiertz, E., and Rapoport, T.A. 2005. Recruitment of the p97 ATPase and ubiquitin ligases to the site of retrotranslocation at the endoplasmic reticulum membrane. *Proc. Natl. Acad. Sci.* **102:** 14132–14138.

Yoshihara, T., Ishigaki, S., Yamamoto, M., Liang, Y., Niwa, J., Takeuchi, H., Doyu, M., and Sobue, G. 2002. Differential expression of inflammation- and apoptosis-related genes in spinal cords of a mutant SOD1 transgenic mouse model of familial amyotrophic lateral sclerosis. *J. Neurochem.* **80:** 158–167.

Zinszner, H., Kuroda, M., Wang, X., Batchvarova, N., Lightfoot, R.T., Remotti, H., Stevens, J.L., and Ron, D. 1998. CHOP is implicated in programmed cell death in response to impaired function of the endoplasmic reticulum. *Genes & Dev.* **12:** 982–995.

FEBS Letters 583 (2009) 213–218

FEBS Letters

journal homepage: www.FEBSLetters.org

Silencing efficiency differs among tissues and endogenous microRNA pathway is preserved in short hairpin RNA transgenic mice

Hiroki Sasaguri [a,c], Tasuku Mitani [b], Masayuki Anzai [b], Takayuki Kubodera [a,c], Yuki Saito [a], Hiromi Yamada [a], Hidehiro Mizusawa [a,c], Takanori Yokota [a,*]

[a] Department of Neurology and Neurological Science, Graduate School, Tokyo Medical and Dental University, 1-5-45 Yushima, Bunkyo-ku, Tokyo 113-8519, Japan
[b] Institute of Advanced Technology, Kinki University, 14-1 Minami-Akasaka, Kainan, Wakayama 642-0017, Japan
[c] Twenty-First Century Center of Excellence Program on Brain Integration and Its Disorders, Tokyo Medical and Dental University, 1-5-45 Yushima, Bunkyo-ku, Tokyo 113-8519, Japan

ARTICLE INFO

Article history:
Received 28 August 2008
Revised 20 November 2008
Accepted 1 December 2008
Available online 11 December 2008

Edited by Ulrike Kutay

Keywords:
RNA interference
Short hairpin RNA
Small interfering RNA
Transgenic mice
MicroRNA
Oversaturation

ABSTRACT

In short hairpin RNA (shRNA) transgenic mice, the tissue difference in gene silencing efficiency and oversaturation of microRNA (miRNA) pathway have not been well assessed. We studied these problems in our previously-reported anti-copper/zinc superoxide dismutase (SOD1) shRNA transgenic mice. Although there was a tissue difference (liver and skeletal muscle, >95%; central nervous system and lung, ~80%), the target gene silencing was systemic and our anti-SOD1 shRNA transgenic mice recapitulated the SOD1-null mice. Neither endogenous miRNAs nor their target gene levels were altered, indicating the preservation of endogenous miRNA pathways. We think that the shRNA transgenic mice can be utilized for gene analysis.

1. Introduction

RNA interference (RNAi) is evolutionally conserved sequence-specific post-transcriptional gene silencing, which is mediated by small double stranded RNA (dsRNA) [1]. The long dsRNA is cleaved by an RNase III enzyme, Dicer, in cytoplasm to generate small interfering RNA (siRNA) that is 21–23 base pair dsRNA. The target mRNA is recognized by guide (antisense) strand of the dsRNA in RNA-induced silencing complex (RISC), and is cleaved by Argonaute-2 (Ago2) protein, one of the main components of RISC [2]. This post-transcriptional gene silencing can be effectively induced by exogenously introduced siRNA or intracellularly expressed short hairpin RNA (shRNA) in mammalian cells [2,3].

The shRNA transgenic mice have been published [4–7] and expected to be an alternative method to the conventional knockout mice. For using shRNA transgenic mice as a tool for gene analysis in vivo, we need to know difference in silencing efficiency among tissues. Moreover, in shRNA transgenic mice, it is also important to elucidate whether microRNA (miRNA) is normally processed, because shRNA and miRNA share intracellular machineries for their maturation in mammalian cells [8–10]. We had generated anti-mouse copper/zinc superoxide dismutase (SOD1) shRNA transgenic mice, in which shRNA was ubiquitously expressed by the RNA polymerase III (Pol III) promoter [11]. Using these mice, we here evaluated the silencing efficiency in various tissues and studied endogenous miRNA pathway.

2. Materials and methods

2.1. Generation of anti-SOD1 shRNA transgenic mice

All experiments were approved by the Animal Experiment Committees of Tokyo Medical and Dental University (#0090104) and Kinki University (KAAT-19-006). We generated an anti-SOD1

Abbreviations: shRNA, short hairpin RNA; miRNA, microRNA; RNAi, RNA interference; dsRNA, double stranded RNA; RISC, RNA-induced silencing complex; Ago2, Argonaute-2; SOD1, copper/zinc superoxide dismutase; Pol III, polymerase III; ES, embryonic stem; PBS, phosphate-buffered saline; SDS, sodium dodecyl sulfate; cDNA, complementary DNA; RT-PCR, reverse transcription polymerase chain reaction; GAPDH, glyceraldehyde-3-phosphate dehydrogenase; snRNA, small nuclear RNA; AAV, adeno-associated virus

* Corresponding author. Fax: +81 3 5803 0169.
E-mail address: tak-yokota.nuro@tmd.ac.jp (T. Yokota).

0014-5793/$34.00
doi:10.1016/j.febslet.2008.12.012